The molecular mechanism for carbon catabolite repression of the chitin response in *Vibrio cholerae*

Virginia E. Green[1], Catherine A. Klancher[1], Shouji Yamamoto[2], Ankur B. Dalia[1,*]

[1]Department of Biology, Indiana University, Bloomington, Indiana, USA
[2]Department of Bacteriology I, National Institute of Infectious Diseases, 162-8640 Tokyo, Japan
*Corresponding author: ankdalia@indiana.edu

ABSTRACT
Vibrio cholerae is a facultative pathogen that primarily occupies marine environments. In this niche, *V. cholerae* commonly interacts with the chitinous shells of crustacean zooplankton. As a chitinolytic microbe, *V. cholerae* degrades insoluble chitin into soluble oligosaccharides. Chitin oligosaccharides serve as both a nutrient source and an environmental cue that induces a strong transcriptional response in *V. cholerae*. Namely, these oligosaccharides induce the chitin sensor, ChiS, to activate the genes required for chitin utilization and horizontal gene transfer by natural transformation. Thus, interactions with chitin impact the survival of *V. cholerae* in marine environments. Chitin is a complex carbon source for *V. cholerae* to degrade and consume, and the presence of more energetically favorable carbon sources can inhibit chitin utilization. This phenomenon, known as carbon catabolite repression (CCR), is mediated by the glucose-specific Enzyme IIA ($EIIA^{Glc}$) of the phosphoenolpyruvate-dependent phosphotransferase system (PTS). In the presence of glucose, $EIIA^{Glc}$ becomes dephosphorylated, which inhibits ChiS transcriptional activity by an unknown mechanism. Here, we show that dephosphorylated $EIIA^{Glc}$ interacts with ChiS. We also isolate ChiS suppressor mutants that evade $EIIA^{Glc}$-dependent repression and demonstrate that these alleles no longer interact with $EIIA^{Glc}$. These findings suggest that $EIIA^{Glc}$ must interact with ChiS to exert its repressive effect. Importantly, the ChiS suppressor mutations we isolated also relieve repression of chitin utilization and natural transformation by $EIIA^{Glc}$, suggesting that CCR of these behaviors is primarily regulated through ChiS. Together, our results reveal how nutrient conditions impact the fitness of an important human pathogen in its environmental reservoir.

AUTHOR SUMMARY
Vibrio cholerae is a facultative human pathogen that most commonly inhabits aquatic environments and can cause the disease cholera when ingested in the form of contaminated food or drinking water. The survival of this pathogen in the marine environment is dependent upon its ability to colonize chitin, an insoluble polysaccharide that is the main constituent of the shells of crustacean zooplankton. *V. cholerae* degrades chitin into soluble oligomers, which can be taken up by this microbe and used as a nutrient. Importantly, chitin oligomers also induce the activity of a chitin-sensing protein, ChiS, to activate the expression of genes required for both (1) eating chitin and (2) undergoing horizontal gene transfer by natural transformation. Previous work demonstrated that more energetically favorable carbon sources, like glucose, can inhibit chitin-induced behaviors. However, the mechanism underlying this response remained unclear. Here, we show how a dephosphorylated intermediate in the glucose uptake pathway – $EIIA^{Glc}$ – interacts with ChiS to repress its activity. Furthermore, we demonstrate that this repression of ChiS by $EIIA^{Glc}$ is responsible for inhibiting both growth on chitin and natural transformation. Together, our results reveal how nutrient conditions impact the fitness of a major human pathogen in its environmental reservoir.

INTRODUCTION
Vibrio cholerae is a Gram-negative, motile bacterium that primarily inhabits marine environments. When ingested, some serogroups are capable of causing the disease cholera, which is characterized by a profuse secretory diarrhea [1]. The differences between the marine environment and the human gut are profound, and *V. cholerae* must express distinct sets of genes in order to survive the challenges specific to each niche [2]. In the marine environment, this organism's expression profile is heavily influenced by contact with chitin, an insoluble polymer of β1,4-linked *N*-acetylglucosamine (GlcNAc) that is found in the shells of crustaceans [3]. *V. cholerae* frequently colonizes and forms biofilms on chitinous surfaces [3, 4]. Chitin oligomers serve as both a nutrient source and an environmental cue that induces the transcription of genes required for efficient chitin catabolism as well as for behaviors that enhance its fitness in this communal setting [3, 5]. These behaviors

include chitin utilization itself as well as natural transformation, a mode of horizontal gene transfer in which bacteria take up exogenous DNA and integrate it into their genomes via homologous recombination [6]. Natural transformation can promote the spread of virulence factors and antibiotic resistance genes in bacterial pathogens [7]. The chitin response is therefore both clinically and ecologically significant for *V. cholerae*. The extracellular degradation of insoluble chitin and subsequent uptake of soluble chitin oligosaccharides is energetically costly; dozens of proteins are required for catabolism, and the enzymes secreted for external digestion may be exploited by cells other than the producer [8, 9]. In contrast, simple six-carbon sugars (i.e., glucose) can enter glycolysis with minimal modification [10]. It may therefore be advantageous for bacteria to consume simple sugars before expending energy to degrade complex polysaccharides like chitin. This hierarchical consumption of sugars is typically achieved through upregulation of genes required to consume the preferred carbon source, repression of genes and proteins involved in catabolism of less preferred carbon sources, or both. This behavior is known as carbon catabolite repression (CCR) [11, 12].

CCR is primarily mediated through proteins of the phosphoenolpyruvate-dependent phosphotransferase system (PTS). This system consists of a broadly conserved set of proteins that mediate a phosphorelay that ultimately facilitates the uptake and concomitant phosphorylation of specific carbohydrates [13]. The first protein in the PTS cascade is Enzyme I (EI). This protein autophosphorylates using the glycolytic intermediate phosphoenolpyruvate (PEP) as a substrate [12]. EI then transfers this phosphate to the histidine phosphocarrier protein (Hpr), which in turn transfers the phosphate to the EIIA domain of a sugar permease complex known as Enzyme II (EII). The EIIA domain can then transfer the phosphate to a cognate EIIB domain, which then transfers the phosphate to the carbohydrate substrate during uptake through the EIIC(D) permease. During substrate import, phosphates flow rapidly through the PTS, skewing the intermediate proteins towards their dephosphorylated states. In the absence of substrate, phosphate flow halts, and the intermediates accumulate in their phosphorylated form [12, 14]. Importantly, this phenomenon means that the phosphorylation status of PTS intermediates reflects the availability of their respective substrates [12, 14]. The relationship between the phosphorylation status of PTS proteins and carbohydrate availability is readily exploited by the cell. PTS intermediates perform a host of regulatory functions that enable careful modulation of cellular processes in response to nutrient availability. These functions depend on the phosphorylation state of PTS intermediates. While many PTS proteins have documented regulatory roles, the central mediator of CCR in Gram-negative bacteria is the glucose-specific Enzyme IIA ($EIIA^{Glc}$), which in *V. cholerae* is responsible for the import of glucose as well as sucrose, trehalose, and *N*-acetylglucosamine [12, 15]. Glucose-induced dephosphorylation of $EIIA^{Glc}$ enables its participation in an array of regulatory activities [12]. Regulation by $EIIA^{Glc}$ has been described for behaviors including metabolism [16], virulence [17], motility [18], and biofilm formation [19]. Understanding the different mechanisms underlying $EIIA^{Glc}$ activity is critical to unraveling how these crucial processes are influenced by carbon availability.

The *V. cholerae* chitin response is among the many behaviors regulated by CCR. *V. cholerae* senses and responds to chitin through the noncanonical hybrid sensor kinase ChiS (chitin sensor) [8]. In the presence of chitin, ChiS activates the transcription of genes required for chitin utilization and natural transformation [8, 20, 21]. However, it has been observed that *V. cholerae* cells grown on $EIIA^{Glc}$-dependent sugars cannot undergo chitin-induced natural transformation [22]. Similarly, strains expressing dephosphorylated $EIIA^{Glc}$ (dephospho-$EIIA^{Glc}$) are non-transformable [23]. The mechanism by which $EIIA^{Glc}$ inhibits this important cellular process is unknown, but a recent study has shown that dephospho-$EIIA^{Glc}$ can reduce ChiS-dependent transcriptional activation [23]. This finding raises the possibility that $EIIA^{Glc}$ inhibition of natural transformation may involve repression of ChiS itself. The mechanism by which dephospho-$EIIA^{Glc}$ represses ChiS is unknown, and it is not clear whether such repression contributes to the previously described CCR of natural transformation [22, 23]. As ChiS also activates the genes required for chitin utilization, it is also possible that dephospho-$EIIA^{Glc}$ will prevent efficient growth on chitin, which is critical for *Vibrio* survival in marine environments [3]. Such regulation might enable *V. cholerae* cells in a chitin-associated biofilm to rapidly take advantage of transiently available sugars (perhaps released from decomposing wildlife).

In this study, we identify the molecular mechanism of CCR of natural transformation and chitin utilization in *V. cholerae*. We find that dephospho-$EIIA^{Glc}$ interacts with ChiS, and that this interaction is required for repression to occur. ChiS suppressor mutations that escape dephospho-$EIIA^{Glc}$-dependent repression also relieve CCR of chitin utilization and natural transformation. Together, these findings suggest that repression of ChiS by dephospho-$EIIA^{Glc}$ is the dominant mechanism of CCR for chitin-dependent responses in *V. cholerae*.

RESULTS

Dephosphorylated EIIA^{Glc} represses ChiS transcriptional activity and downstream behaviors

ChiS activity can be assessed through its direct activation of the chitobiose utilization operon (*chb*) [8, 24]. In the presence of chitin, ChiS strongly activates this locus, resulting in the transcription of genes required for the uptake and utilization of chitobiose [8]. In the absence of chitin, ChiS is repressed by the periplasmic chitin binding protein (CBP). Previous work has shown that the deletion of CBP is sufficient to genetically activate ChiS even in the absence of chitin [8]. We therefore used a P_{chb}-*GFP* transcriptional reporter [25] in a Δ*cbp* background to interrogate ChiS activity. Consistent with previous findings [23], we observed that rendering EIIA^{Glc} dephosphorylated by the deletion of its upstream phosphate donor EI represses ChiS transcriptional activity (**Fig. 1A**). This repression can be relieved by the simultaneous deletion of EIIA^{Glc}, suggesting that EIIA^{Glc} plays a critical role in this repression (**Fig. 1A**). We generated a genetically locked dephospho-EIIA^{Glc} allele [26] by mutating the phosphorylated histidine to a glutamate (H91Q) and found that this allele was sufficient to repress ChiS activity in a background where EI was intact (**Fig. 1A**). Furthermore, a proposed phosphomimetic EIIA^{Glc} H91D allele [19] cannot repress ChiS in a ΔEI background. All together, these results are consistent with a model in which dephospho-EIIA^{Glc} represses ChiS activity (**Fig. 1A**).

These findings suggested that the phosphorylation status of EIIA^{Glc} is central to its ability to repress ChiS activity. Phosphorylated EIIA^{Glc} stimulates the activity of adenylate cyclase to increase the cellular levels of the second messenger cyclic AMP (cAMP), while dephospho-EIIA^{Glc} cannot promote this activity [12, 27-29]. ChiS-dependent activity requires cAMP, as evidenced by the fact that an adenylate cyclase mutant displays no induction of P_{chb} unless exogenous cAMP is supplied (**Fig. S1A**). Because the deletion of EIIA^{Glc} markedly rescues ChiS activity, we reasoned that low cAMP levels were not the primary mechanism for ΔEI repression of ChiS since ΔEI ΔEIIA^{Glc} mutants and ΔEI mutants both lack phosphorylated EIIA^{Glc} for stimulating adenylate cyclase activity. However, to formally test this, we performed assays in the presence and absence of supplemental cAMP. Consistent with previous reports [23], cAMP is unable to rescue ChiS activity in the ΔEI or EIIA^{Glc} H91Q backgrounds (**Fig. S1A**). Thus, EIIA^{Glc} is repressing ChiS activity via a mechanism other than through the indirect regulation of adenylate cyclase activity because cAMP cannot rescue ChiS activity while dephospho-EIIA^{Glc} is present in the cell.

Our previous experiments utilized a Δ*cbp* mutation to genetically induce ChiS activity in the absence of chitin. Therefore, we next asked whether repression by EIIA^{Glc} affects ChiS transcriptional activity in a more physiologically relevant setting. To test this question, we grew cells containing a P_{chb}-*mCherry* reporter [25] on insoluble chitin for 48 hours and assessed fluorescence of individual cells using microscopy. The mCherry signal was normalized to a constitutively expressed GFP construct to account for internal noise in gene expression. Importantly, these strains all had *cbp* intact, which allows for natural chitin-induced activation of ChiS. As expected, parent cells robustly activated the P_{chb}-*mCherry* reporter under these conditions, while cells lacking ChiS did not (**Fig. 1B**). The ΔEI mutation significantly repressed ChiS activity in this assay (**Fig. 1B**). This repression could be fully relieved by the tandem deletion of EIIA^{Glc} (**Fig. 1B**), mirroring what was observed when the Δ*cbp* mutation was used to induce ChiS activity (**Fig. 1A**). Interestingly, the nonphosphorylatable EIIA^{Glc} H91Q allele only slightly repressed ChiS in this assay (**Fig. 1B**). This result suggests that EIIA^{Glc} H91Q may be a less potent repressor of ChiS than natural dephospho-EIIA^{Glc}, which is more readily observed when ChiS activity is stimulated via natural chitin induction. The reduced efficacy of the H91Q allele might be explained by the fact that for other targets of EIIA^{Glc}, the H91 residue is part of the protein-protein binding interface [30-33]. Thus, beyond affecting phosphorylation, mutations to this residue may affect the ability of EIIA^{Glc} to interact with its downstream targets, which may include ChiS. Lastly, the phosphomimetic EIIA^{Glc} H91D [19] allele mediated no repression of ChiS in the ΔEI background (**Fig. 1B**), further supporting that dephospho-EIIA^{Glc} inhibits ChiS activity. Once again, exogenous addition of cAMP was unable to rescue ChiS activity in the ΔEI background (**Fig. 1B, Fig. S1B**). Interestingly, the addition of cAMP did restore P_{chb} expression in the ΔEI/EIIA^{Glc} strain back to parent levels of activity (**Fig. S1B**), suggesting that a reduction of cAMP in this background (due to low adenylate cyclase activity in the absence of phosphorylated EIIA^{Glc}) does play a small role in limiting ChiS transcriptional activity. Together, these results support our previous observations and reaffirm that EIIA^{Glc} inhibits ChiS activity in physiologically relevant conditions.

Having observed a strong repressive effect on ChiS-dependent transcription, we sought to determine whether EIIA^{Glc} repression impacts ChiS-controlled behaviors. ChiS directly activates the genes required for chitin uptake and catabolism [3, 8, 24]. We therefore asked whether dephospho-EIIA^{Glc} affects the ability of *V. cholerae* to grow on insoluble chitin over 72 hr. We found that deletion of EI reduced final growth yield to the same level as a ChiS deletion (**Fig. 1C**). This defect in growth yield was restored in the ΔEI ΔEIIA^{Glc} double mutant (**Fig. 1C**). Growth yield was only partially reduced by EIIA^{Glc} H91Q, which is consistent with the

intermediate repression mediated by this allele on chitin-induced ChiS activity. EIIA^{Glc} H91D relieved the repressive effects of the ΔEI mutation on growth yield (**Fig. 1C**). Once again, exogenous cAMP did not alter these outcomes (**Fig. S2**). These results suggest that EIIA^{Glc}-mediated repression of ChiS activity is sufficient to repress the ability of *V. cholerae* to use insoluble chitin as a carbon source.

Apart from regulating chitin utilization, ChiS is also essential for the induction of natural transformation [5, 20, 21], a physiological state in which cells are able to take up extracellular DNA from the environment to incorporate into their genome by homologous recombination [6]. Consistent with previous work, we found that while parent cells transform at a high frequency, transformation is significantly impaired in a ΔEI background [23] (**Fig. 1D**). However, in contrast with previous work [23], we observed a partial rescue in transformation in the ΔEI ΔEIIA^{Glc} double mutant. We attribute this discrepancy to differences in the dynamic ranges of our transformation assays; the reduced transformation frequency of the ΔEI ΔEIIA^{Glc} strain likely falls below the limit of detection of the less sensitive assay used to previously test this question. Interestingly, the EIIA^{Glc} H91Q mutant displayed a subtle but statistically significant transformation defect (**Fig. 1D**). Our findings above indicate that this allele is likely a less effective repressor of ChiS activity compared to natural dephospho-EIIA^{Glc}. Previous work from our lab has also shown that strains that exhibit growth defects on chitin can still transform at high levels, suggesting that the threshold of chitin induction required for cells to transform may be lower than that required for growth on chitin [34]. This may explain why the EIIA^{Glc} H91Q mutant exhibited a subtle transformation defect (**Fig. 1D**). The phosphomimetic EIIA^{Glc} H91D mutation in the ΔEI background transformed at parent levels, which further suggests that dephospho-EIIAGlc is required for inhibition of natural transformation in the ΔEI background (**Fig. 1D**). As seen in the previous assays, cAMP was unable to restore transformation of the ΔEI mutant to parent levels (**Fig. S3**). All together, these results indicate that dephospho-EIIA^{Glc} significantly impairs ChiS transcriptional activity and downstream behaviors (*i.e.*, growth on chitin and chitin-induced natural transformation), in a cAMP-independent manner.

Dephosphorylated EIIA^{Glc} inhibits ChiS DNA-binding activity

We next wanted to probe the mechanism by which EIIA^{Glc} represses ChiS activity. ChiS has a DNA-binding domain and directly binds to the *chb* promoter [24, 35]. Thus, we hypothesized that EIIA^{Glc} might interfere with ChiS DNA-binding. To test this possibility, we performed chromatin immunoprecipitation (ChIP)-qPCR assays using a previously characterized functional [24] FLAG-tagged construct of ChiS to assess DNA-binding *in vivo*. We hypothesized that if dephospho-EIIA^{Glc} inhibits DNA binding, ChiS should no longer be able to ChIP the *chb* promoter; however, if dephospho-EIIA^{Glc} inhibits activation downstream of DNA binding, we should still observe ChiS DNA-binding in a ΔEI mutant. When we performed this experiment, we observed that ChiS DNA binding is inhibited in a ΔEI mutant but rescued in the ΔEI ΔEIIA^{Glc} mutant. These data suggest that dephospho-EIIA^{Glc} inhibits the DNA-binding activity of ChiS (**Fig. 2**).

ChiS interacts with dephosphorylated EIIA^{Glc}.

We next sought to determine the mechanism by which dephospho-EIIA^{Glc} represses ChiS DNA-binding activity. EIIA^{Glc} has been shown to regulate many target proteins through protein-protein interactions, in a manner that can either stimulate or inhibit the activity of those interacting partners [16, 30, 36, 37]. We therefore hypothesized that dephospho-EIIA^{Glc} might interact with ChiS to repress its activity. To test whether EIIA^{Glc} and ChiS interact, we first assessed whether these proteins colocalized *in vivo*. Specifically, we generated cells that express an EIIA^{Glc}-mCherry fusion that can still repress ChiS (**Fig. S4**) and an inducible GFP-tagged construct of ChiS [24], and examined their cellular localization pattern using fluorescence microscopy. We observed that when we did not induce ChiS-GFP, EIIA^{Glc}-mCherry was diffuse throughout the cytoplasm (**Fig. 3**). When we overexpressed ChiS in cells where EI is intact, EIIA^{Glc} remained diffuse in 90% of cells, while in 10% of cells, ChiS and EIIA^{Glc} formed colocalized foci (**Fig. 3**). Strikingly, when we deleted EI (rendering all EIIA^{Glc} within the cell dephosphorylated), the percentage of cells containing colocalized ChiS-EIIA^{Glc} foci increased to 90% (**Fig. 3**). Furthermore, 81% of cells expressing EIIA^{Glc} H91Q displayed colocalizing foci (**Fig. 3**), further suggesting that dephospho-EIIA^{Glc} interacts with ChiS. Consistent with this hypothesis, only 4% of cells expressing the phosphomimetic EIIA^{Glc} H91D allele in a ΔEI background display colocalizing foci.

Colocalization of proteins *in vivo* only indicates that they are occupying a similar subcellular site and cannot independently confirm that they interact. We therefore wanted to test whether the colocalization observed between ChiS and EIIA^{Glc} was the result of an interaction. To this end, we took advantage of the PopZ-linked apical recruitment (POLAR) assay [38]. In this assay, two putative interaction partners – the "bait" and "prey" - are fluorescently tagged. The bait is also tagged with an H3H4 PopZ oligomerization domain. The H3H4 domain specifically interacts with the PopZ protein from *Caulobacter crescentus*, which localizes to cell

poles when heterologously expressed in other bacterial species [39]. Thus, when PopZ is expressed in cells it relocalizes the bait to the cell poles. If the bait and prey interact, PopZ-dependent relocalization of the bait should cause a concomitant relocalization of the prey to the cell poles. However, if the bait and prey do not interact, PopZ-dependent relocalization of the bait should not alter the localization of the prey. Thus, to test if ChiS and EIIA^{Glc} interact, we generated cells with ChiS-H3H4-msfGFP as the bait and EIIA^{Glc}-mCherry as the prey. In the absence of PopZ, ChiS and EIIA^{Glc} foci localize both to the cell poles and midcell (**Fig. 3C**). When PopZ is induced, the ChiS bait relocalizes to the cell poles as expected (**Fig. 3C**). Consistent with ChiS and EIIA^{Glc} interacting, nearly all EIIA^{Glc} foci are relocalized to the cell poles when PopZ is induced (**Fig. 3C**). Together, these results strongly suggest that ChiS and dephospho-EIIA^{Glc} interact.

To further test this interaction, we also performed *in vivo* pulldowns using the functional ChiS-FLAG and EIIA^{Glc}-mCherry alleles. To stabilize protein-protein interactions, the crosslinker disuccinimidyl suberate (DSS) was added to cells prior to performing the pull down. To test whether ChiS interacts with EIIA^{Glc} in a phosphorylation-dependent manner, we performed pulldowns of ChiS-FLAG in strains where EI was intact vs deleted. We observed that when EI was intact, no EIIA^{Glc}-mCherry could be detected in the elution fraction (**Fig. 3D**). However, when EI was deleted, a high molecular weight band was detected in the EIIA^{Glc}-mCherry elution fraction, consistent with an interaction between EIIA^{Glc} and ChiS (**Fig. 3D**). This band was not detected in the absence of ChiS, even if EI was deleted (**Fig. 3D**). Importantly, we confirmed that dephospho-EIIA^{Glc} represses ChiS activity in the same strains and conditions used for these pulldown assays using the P$_{chb}$-*GFP* reporter (**Fig. S5**). These results further indicate that ChiS and dephospho-EIIA^{Glc} interact.

Isolation of ChiS suppressor alleles that cannot be inhibited by dephosphorylated EIIA^{Glc}

The genotypes that promote ChiS-EIIA^{Glc} interactions (e.g., ΔEI and EIIA^{Glc} H91Q) correlate with the genotypes in which EIIA^{Glc} represses ChiS activity (**Fig. 1A-D, Fig. 3**). We therefore hypothesized that this interaction is required for EIIA^{Glc} to inhibit ChiS. To test this possibility, we took an unbiased approach by isolating ChiS suppressor mutants that can escape EIIA^{Glc}-dependent inhibition and then tested these alleles for their ability to interact with EIIA^{Glc}. To isolate ChiS suppressor mutants, we used error-prone PCR to randomly mutagenize ChiS and introduced these mutated alleles into a Δ*cbp* ΔEI (*i.e.*, dephospho-EIIA^{Glc}) strain containing a previously described P$_{chb}$-*lacZ* reporter [25, 40]. We screened ~5,500 colonies for the recovery of ChiS activity as indicated by blue colonies on X-gal plates. Of the suppressor mutations we isolated, two were able to fully rescue ChiS transcriptional activity in a ΔEI background: W388C and I429T (**Fig. 4**). Both suppressor alleles significantly rescued transcriptional activity using either Δ*cbp* or insoluble chitin to induce ChiS activity in the ΔEI background (**Fig. 4A-B**). This rescue was similar to that conferred by the deletion of EIIA^{Glc} (ΔEI ΔEIIA^{Glc}) (**Fig. 4A-B**). Furthermore, deleting EIIA^{Glc} did not further increase the activity of these suppressor alleles in the ΔEI background, implying that the ChiS suppressor mutations and EIIA^{Glc} are epistatic and work via the same pathway (**Fig. 4A-B**). Consistent with transcriptional activity, dephospho-EIIA^{Glc} failed to inhibit the DNA-binding activity of both ChiS suppressor alleles *in vivo* (**Fig. 2**). Importantly, the expression level of both ChiS suppressor mutants is comparable to the WT in a ΔEI background, suggesting that an increased abundance of ChiS cannot account for the phenotypes observed (**Fig. S6**).

We also tested the ability of CBP to repress both ChiS suppressor alleles. Like native ChiS, ChiS^{W388C} was fully repressed by CBP (**Fig. 4A**). ChiS^{I429T} had observable activity in the presence of CBP, but its activity was still significantly increased when CBP was deleted (**Fig. 4A**). This finding suggests that ChiS^{I429T} can still be repressed by CBP, but not as efficiently as native ChiS. Together, these data suggest that the W388C and I429T mutations render ChiS specifically resistant to repression by dephospho-EIIA^{Glc}.

Because these suppressor alleles restored ChiS transcriptional activity in the ΔEI mutant, we next tested whether they also rescue the ChiS-dependent phenotypes of chitin utilization and natural transformation from ΔEI repression. We found that both suppressor mutations significantly rescued both chitin utilization (**Fig. 4C**) and natural transformation (**Fig. 4D**). These data suggest that the repression of these behaviors by the ΔEI mutation is largely mediated through EIIA^{Glc}-dependent repression of ChiS activity. Furthermore, these outcomes were largely unaffected by the addition of cAMP, suggesting that dephospho-EIIA^{Glc}-dependent repression of ChiS activity is the primary mechanism of CCR in the ΔEI background (**Fig. S2-S3**).

ChiS suppressor alleles no longer interact with dephosphorylated EIIA^{Glc}

We previously showed that dephospho-EIIA^{Glc} and ChiS colocalize *in vivo* (**Fig. 3**). We hypothesized that if EIIA^{Glc} needs to interact with ChiS to inhibit its activity, then the ChiS suppressor mutants would no longer be able to interact with dephospho-EIIA^{Glc}. Indeed, we found that these ChiS suppressor alleles (W388C and I429T) significantly reduced the colocalization of ChiS with dephospho-EIIA^{Glc} when compared to the ChiS

parent (**Fig. 5A-B**). Furthermore, dephospho-EIIA^{Glc}-mCherry no longer co-immunoprecipitated with ChiS^{W388C}-FLAG (**Fig. 5C**). These data strongly indicate that EIIA^{Glc} must interact with ChiS to repress its activity.

The ChiS^{W388C} suppressor allele confers resistance to glucose-induced CCR of natural transformation

Thus far, we have induced CCR via genetics means (i.e., via use of ΔEI or EIIA^{Glc} H91Q mutations) to show that dephospho-EIIA^{Glc} inhibits ChiS activity. We next sought to test CCR of ChiS using carbon sources that naturally induce CCR. It was previously shown that glucose inhibits natural transformation in *V. cholerae* [5, 22]. Because cAMP/CRP are critical for induction of natural transformation in conjunction with the master competence regulator TfoX [41, 42], this inhibition was previously assumed to be due to the reduction of cAMP resulting from the dephosphorylation of EIIA^{Glc} by glucose [41-44]. We observed that while cAMP does increase transformation in a ΔEI strain, transformation is increased further by the deletion of EIIA^{Glc} (**Fig. S3**). Furthermore, deletion of EIIA^{Glc} is sufficient to increase transformation even in the absence of exogenous cAMP (**Fig. S3**). Therefore, we hypothesized that the dominant mechanism for CCR of natural transformation by glucose is through the repression of ChiS activity by dephospho-EIIA^{Glc}. To test this, we compared the transformation efficiency of a strain with ChiS^{WT} to a strain with ChiS^{W388C} in the presence of glucose to induce CCR. As previously reported, glucose inhibited transformation of our parent strain (i.e., harboring ChiS^{WT}) [5, 22] (**Fig. S7A**). However, contrary to our initial hypothesis, we found that transformation of ChiS^{W388C} was also inhibited by glucose (**Fig. S7A**). Furthermore, the addition of exogenous cAMP did not rescue transformation in either strain background when glucose was present (**Fig. S7A**). This is in contrast to the rescue conferred by exogenous cAMP on the transformation frequency of a mutant lacking adenylate cyclase (**Fig. S3**).

One possible explanation for these results is that catabolism and growth of cells on glucose during these transformation assays inhibits transformation nonspecifically—for example, through dilution of the machinery required for DNA uptake and integration during rapid cell division. If this hypothesis is true, other supplemental carbon sources should be similarly repressive—even if they are not imported by the PTS (and therefore, would not activate a canonical CCR response). To test this, we assessed transformation efficiency in the presence of fructose (a PTS sugar that uses a separate EIIA protein), maltose (an ABC transported sugar), and a mixture of glutamate and proline. We found that all carbon sources significantly inhibited the transformation of both ChiS^{WT} and ChiS^{W388C} regardless of whether exogenous cAMP was provided (**Fig. S7A**). These data suggest that the growth of cells in the presence of an additional carbon source (whether it can induce CCR or not) confounds our ability to assess the role of CCR in repressing ChiS using natural substrates. We therefore devised a strategy to separate the effects of glucose induction of CCR from its downstream metabolism. Phosphoglucoisomerase (PGI) is responsible for converting glucose-6-phosphate into fructose-6-phosphate during glycolysis. Thus, ΔPGI mutants can still take up glucose via the PTS but lack the ability to catabolize it (**Fig. S8**). When we tested the transformation of a ΔPGI mutant, we found that it maintained the ability to transform. However, this transformation was fully inhibited by glucose in cells with ChiS^{WT}. By contrast, ΔPGI cells with ChiS^{W388C} were highly transformable (**Fig. 6**). Once again, these phenotypes were not affected by cAMP (**Fig. S7B**). These data suggest that glucose uptake causes CCR of natural transformation, and that the dominant mechanism for this repression is via EIIA^{Glc}-dependent inhibition of ChiS activity.

We next asked whether CCR of ChiS by EIIA^{Glc} was specific to the E7946 strain of *V. cholerae* used throughout this study or if it was a conserved response. Specifically, we tested the ability of dephospho-EIIA^{Glc} to repress ChiS activity in our chitin-induced reporter assay in two other toxigenic *V. cholerae* strains (C6706 [45], A1552 [46]) as well as a nontoxigenic, non-O1/O139 environmental isolate strain (CR03-424 [47]). Furthermore, we tested this response in the more distantly related species *Vibrio campbellii* DS40M4 [48, 49]. In all strains tested, we observed ChiS-dependent activation of P_{chb}-*mCherry* in response to chitin (**Fig. S9**). Furthermore, we observed a significant decrease in activation upon the deletion of EI, which could be rescued by the simultaneous deletion of EIIA^{Glc} (**Fig. S9**). These results demonstrate that dephospho-EIIA^{Glc}-dependent CCR of ChiS is a conserved response in these systems.

DISCUSSION

In this study, we uncover the molecular mechanism responsible for CCR of chitin-dependent responses in *V. cholerae* (**Fig. 7**). We show that dephospho-EIIA^{Glc} interacts with ChiS *in vivo* to repress its DNA-binding activity, resulting in the inhibition of chitin utilization and natural transformation. These results reveal a novel mechanism by which carbon availability regulates natural competence and illuminate *Vibrio cholerae* regulation of these critical behaviors in response to nutrient conditions.

Given their energetic cost, it is not surprising that both chitin utilization and natural transformation are tightly regulated processes. Multiple regulators have been identified for ChiS alone [8, 25, 40]. The conservation of a pathway for regulation of these behaviors by PTS sugars raises the question of where *V. cholerae* cells might encounter such sugars while the chitin response is active. In the context of a chitin-associated biofilm, the ability to rapidly inhibit the chitin response to take advantage of favorable carbon sources (perhaps released from decomposing wildlife) might provide a considerable advantage. Alternatively, it is possible that when this pathogen is ingested, the rapid shutdown of the chitin response within the host gut might aid in colonization. While the primary product of chitinolytic activity is the chitin disaccharide chitobiose, a minor amount of GlcNAc, the monosaccharide subunit of chitin, may be produced [50]. PTS-mediated uptake of GlcNAc should also render $EIIA^{Glc}$ dephosphorylated. Thus, the uptake of GlcNAc liberated via chitinolytic activity may serve as a negative feedback mechanism to inhibit the chitin response [15].

While it is easy to speculate that glucose inhibits chitin utilization to maximize efficiency in carbon metabolism, the link between carbon availability and natural transformation is less intuitive. In *V. cholerae*, natural transformation and chitin utilization are inextricably linked due to their activation by ChiS. It is possible that a survival advantage is primarily conferred by the ability to regulate chitin utilization, and that the regulation of natural transformation is a by-product. However, this hypothesis is challenged by data from *Haemophilus influenzae*, where natural competence is similarly inhibited by favorable sugars [51]. Furthermore, in *H. influenzae, V. cholerae, and Bacillus subtilis*, the induction of competence coincides with a stressful and nutrient-poor environment [5, 51, 52]. If competence is beneficial to species in stressful environments, the appearance of favorable carbon sources may lessen the need for such a response.

On a mechanistic level, this study also expands our understanding of how CCR regulates natural transformation. Work in *V. cholerae* has attributed CCR of natural transformation solely to the low cAMP levels that result from sugar-induced $EIIA^{Glc}$ dephosphorylation [22]. We observed that while modulation of intracellular cAMP does play a minor role, the $EIIA^{Glc}$-mediated repression of ChiS activity represents the dominant mechanism for CCR of chitin-induced behaviors in *V. cholerae*. This finding differs from CCR of natural transformation in *H. influenzae*, where fructose-mediated repression can be completely relieved by the addition of exogenous cAMP [51]. The additional layer of regulation present in *V. cholerae* is striking, and as discussed above, may have evolved as a response to the system's unique mode of competence induction. The direct regulation by $EIIA^{Glc}$ may strengthen the cell's control over this costly response by rapidly and efficiently preventing its activation in the presence of favorable carbon sources.

This study also adds another member to the extensive $EIIA^{Glc}$ regulon. The ability of $EIIA^{Glc}$ to physically interact with diverse binding partners is poorly understood. Contributing an additional binding partner has the potential to help define requirements for regulation by $EIIA^{Glc}$, thereby expanding our understanding of how this versatile protein controls a number of key biological processes [19, 53-56].

ChiS is a membrane-embedded hybrid sensor kinase. When chitin oligomers enter the periplasm, they trigger a conformational change in ChiS that is transmitted from its periplasmic domain through a transmembrane domain [8, 24]. This transmembrane domain connects to a flexible linker domain known as a HAMP (present in Histidine kinases, Adenylate cyclases, Methyl-accepting proteins, and Phosphatases) domain, which in turn propagates the signal to the cytoplasmic portion of the protein to activate DNA binding [8, 24]. Interestingly, the W388C suppressor mutation is located within the HAMP domain. The I429T suppressor mutation is located directly after the end of the HAMP domain, but before the beginning of the next domain. We hypothesize that these mutations likely confer resistance to repression in one of two ways. First, they may lie at a binding interface between ChiS and $EIIA^{Glc}$, preventing hydrophobic or electrostatic interactions typically required for effective repression. Or second, they may trigger a conformational change in the downstream domains of the protein such that the true binding interface becomes inaccessible to $EIIA^{Glc}$. Interestingly, a single mutation within a HAMP domain has previously been shown to constitutively activate the downstream sensor kinase [57]. The ability of single mutations in the HAMP to drastically alter downstream protein conformation may lend support to the latter hypothesis. Regardless of their mechanism of action, these ChiS suppressor alleles were integral to test the importance of $EIIA^{Glc}$-dependent repression of ChiS activity on CCR of chitin-induced behaviors in *V. cholerae*.

Lastly, our findings also expand our understanding of the mechanisms by which organisms execute CCR. CCR is a widespread mode of gene regulation in diverse bacterial species. Typically, it involves the repression of proteins directly involved in the process being regulated (often permeases or kinases) [12, 30, 32, 56, 58]. In Firmicutes, regulation of transcription factors through protein-protein interactions is also extremely common [59]. However, CCR of transcription factors is less established in Gram-negative organisms [18, 59]. Interestingly, a recent study in *Vibrio vulnificus* identified a transcription factor that can be activated by

a direct interaction with dephospho-EIIA^{Glc} [37]. This result coupled with our findings may suggest that EIIA^{Glc}-dependent regulation of transcription factors is conserved in Gram-negative microbes.

METHODS

Bacterial strain and culture conditions

Mutant strains were derived from *Vibrio cholerae* E7946 [60]. Unless otherwise indicated, strains were grown in LB Miller broth at 30°C rolling and on LB Miller agar. When necessary, LB was supplemented with kanamycin at 50 µg/mL, trimethoprim at 10 µg/mL, spectinomycin at 200 µg/mL, chloramphenicol at 1 µg/mL, carbenicillin at 100 µg/mL, or zeocin at 100 µg/mL.

Strain Construction

Mutant constructs were created using splicing by overlap extension (SOE) PCR as previously described [61]. Constructs were introduced into strains using natural transformation, either chitin-induced [62] or genetically induced using an IPTG-inducible *tfoX* plasmid (pMMB67EH-*tfoX*). In all cases, this plasmid was cured before the strains were used in experiments. Constructs were verified by PCR and/or sequencing (all point mutations and in-frame deletions were verified by sequencing). All genes referenced in this study and their corresponding identifiers within the *Vibrio cholerae* genome can be found in **Table S1**. All strains used in this study can be found in **Table S2**. Gene deletions were in-frame unless otherwise indicated. For a list of primers used in this study, see **Table S3**.

GFP ChiS Activity Assays

GFP assays were performed almost exactly as previously described [24]. Briefly, strains were streaked from frozen stocks onto LB agar and grown at 30°C overnight. Single colonies were then picked into LB broth and grown rolling overnight for 17 hours at 30°C. Overnight cultures were washed and resuspended to an OD_{600} of 3.0 in Instant Ocean (IO; 7g/L, Aquarium Systems). The GFP fluorescence (excitation: 500 nm; emission: 540 nm) of 200 µL of this resuspension was assessed using a BioTek H1M plate reader. Background fluorescence was determined by assaying a non-fluorescent strain in each assay and was subtracted from all samples.

Chitin-Induced ChiS Activity Assays

Strains were inoculated from frozen stocks into LB broth and grown rolling overnight at 30°C. Overnight cultures were then washed and resuspended in IO. 10^8 cells suspended in 100 µL of IO were then mixed with 1 mL chitin reactions including 150 µL chitin slurry (53 g chitin powder / L IO), 565 µL IO, and either 185 µL cAMP (5 mM final concentration) or an equal volume of water. Reactions were incubated shaking for 48 hours at 30°C. Cells were then removed from the chitin by vortexing, suspended in Instant Ocean, and placed on a glass coverslip beneath a 0.2% IO gelzan pad. Cells were imaged using an inverted Nikon Ti-2 microscope with a Plan Apo 60x objective lens, FITC (excitation: 470 nm; emission: 535 nm) and mCherry (excitation: 575 nm; emission: 635 nm) filter cubes, a Hamamatsu ORCAFlash 4.0 camera, and Nikon NIS Elements imaging software. Average fluorescence per cell was quantified using Fiji [63] and the MicrobeJ [64] plugin. The background fluorescence was determined by imaging a non-fluorescent strain and subtracted from samples. To account for internal noise in gene expression, reporter fluorescence was normalized to a constitutively expressed GFP construct. For each biological replicate, the geometric mean was calculated from ~200 individual cells.

Insoluble Chitin Growth Curves

Strains were inoculated from frozen stocks into LB broth and grown rolling overnight at 30°C. Overnight cultures were washed and resuspended in M9 minimal media (1X M9 salts + 2 mM $MgSO_4$ + 30 µM $FeSO_4$ + 0.1 mM $CaCl_2$). 10^4 cells suspended in 10 µL of M9 were then added to 1 mL chitin reactions containing 150 µL chitin slurry, 655 µL M9 minimal media, and either 185 µL cAMP (5 mM final concentration) or an equal volume of water. Growth reactions were grown shaking at 30°C for 72 hours. Quantitative dilution plating was performed at 0, 24, 48, and 72 hours.

Transformation Assays

Strains were inoculated from frozen stocks into LB broth and grown rolling overnight at 30°C. Overnight cultures were subcultured and grown to an OD_{600} of 0.5-1.0. Subcultured cells were washed and resuspended in IO, and 10^8 cells suspended in 100 µL IO were mixed with 1 mL chitin reactions including 150 µL chitin slurry, 565 µL IO, either 185 µL cAMP (5 mM final concentration) or an equal volume of water, and, when

applicable, 0.5% final concentration of either glucose, fructose, maltose, or a cocktail of glutamate and proline. Cells were incubated static at 30°C for ~18 hours. Then, 550 µL of supernatant was removed from the reactions, and 500 ng of purified transforming DNA (tDNA) was mixed with the cells by light vortexing. The tDNA replaced a frame-shifted transposase gene with a chloramphenicol resistance marker (*i.e.*, ΔVC1807::Cm^R). DNA and cells were incubated for 5 hours static at 30°C. Reactions were then outgrown by adding 500 µL LB broth and shaking at 37°C for 2 hrs. Reactions were then plated for quantitative culture on both plain LB agar (total viable counts) and LB agar + chloramphenicol (1 µg/mL) (transformants). Transformation frequency was calculated by dividing the number of transformants by the total viable counts.

Colocalization Microscopy

Strains were inoculated from frozen stocks into LB broth + 20 µM IPTG to induce the P_{tac}-*chiS-msfGFP* constructs and grown rolling overnight at 30°C. For POLAR experiments, strains were supplemented with 0.2% arabinose to induce P_{BAD}-PopZ. Overexpression of ChiS induces a strong cell curving phenotype in *Vibrio cholerae* for reasons that remain unclear. Because this curvature disrupts polar relocalization and downstream analysis, we deleted the *crvA* gene, which is required for cell curvature in *V. cholerae*, for the strain used in this assay [65]. Overnight cultures were washed and resuspended to an OD_{600} of 0.3 in IO and placed on a glass coverslip beneath a 0.2% IO gelzan pad. Cells were imaged using the Nikon Ti-2 microscope discussed above. GFP and mCherry foci were visualized on Fiji [63] and 100 cells were analyzed per replicate for a total of ≥300 cells per sample. Heat maps were generated using Fiji and the MicrobeJ plugin [64].

Protein Co-Immunoprecipitation

Strains containing a P_{tac}-*chiS-FLAG* allele and natively expressed $EIIA^{Glc}$-mCherry were inoculated from colonies streaked on LB agar into 50 mL flasks of LB broth supplemented with 1 µM IPTG (to induce P_{tac}-*chiS-FLAG*). Flasks were grown shaking at 30°C for 24 hr. Cultures were then crosslinked with 1 mM disuccinimidyl suberate (DSS) for 30 minutes at room temperature shaking before being quenched with 100 mM Tris for 20 minutes at room temperature shaking. Quenched samples were washed twice with coIP buffer 1 (50 mM Tris-Cl pH 7.4, 150 mM NaCl, 1 mM EDTA) and then stored at -80°C. Frozen pellets were resuspended in 1 mL coIP buffer 2 (50 mM Tris-Cl pH 7.4, 150 mM NaCl, 1 mM EDTA, 10 mM $MgCl_2$, 1% triton, 2% glycerol). Cells were then lysed by the addition of 1x Fastbreak cell lysis reagent (Promega), 1x protease inhibitor cocktail [100x inhibitor cocktail contained the following: 0.07 mg/mL phosphoramidon (Santa Cruz), 0.006 mg/mL bestatin (MPbiomedicals/Fisher Scientific), 1.67 mg/mL AEBSF (Gold Bio), 0.07 mg/mL pepstatin A (DOT Scientific), 0.07 mg/mL E64 (Gold Bio) suspended in DMSO], 250 µg/mL lysozyme, and 500 units/mL benzonase nuclease (Sigma) for 30 mins rocking at room temperature. Lysates were clarified by centrifuging at 10,000 x g for 10 minutes at 4°C. Then, 50 µL of clarified lysate was mixed with 50 µL 2x SDS PAGE sample buffer (200 mM Tris pH 6.8, 25% glycerol, 1.8% SDS, 0.02% Bromophenol Blue, 5% β-mercaptoethanol) to serve as the "protein input" sample. 1 mL of lysate was then added to 100 µL Pierce anti-DYKDDDDK magnetic agarose equilibrated in coIP buffer 2. The lysate was incubated with the agarose for 2hr at 4°C with end-over-end mixing. Supernatant was then removed using a magnetic separation rack and discarded. The agarose was then washed three times with 500 µL coIP buffer 2 for 10 minutes rocking and then briefly washed one additional time in 500 µL coIP buffer 2. Protein was then eluted off the agarose by resuspension in 100 µL of 3X FLAG elution buffer (3 µL of 5 mg/mL Sigma 3X FLAG peptide solution + 97 µL of coIP buffer 2) followed by 30 minutes of rocking at room temperature. Eluant was collected using a magnetic separation rack and was mixed 1:1 with 2x SDS PAGE sample buffer to serve as "protein elution" sample. All samples were then boiled for 10 minutes. For visualizing ChiS-FLAG, 5 µL of input sample or 15 µL of elution sample were separated on a 7.5% SDS PAGE gel. For visualizing $EIIA^{Glc}$-mCherry, 5 µL of input sample or 15 µL of elution sample were separated on a 15% SDS PAGE gel. Following separation, proteins were electrophoretically transferred to a PVDF membrane. Membranes were then blocked for at least 1 hour in 5% milk and then incubated overnight rocking with either rabbit polyclonal α-FLAG (1:1000, Sigma) or rabbit polyclonal α-mCherry (1:10,000, ThermoFisher). Membranes were then washed and incubated for at least 2 hours with α-rabbit horseradish peroxidase-conjugated secondary antibodies (1:10,000). Membranes were then washed and incubated with both primary and secondary antibodies again to maximize signal. Blots were then washed and probed with Pierce ECL Western Blotting Substrate. Blots were imaged with a ProteinSimple FluorChem R system.

Chromatin Immunoprecipitation Assays

ChIP assays were performed almost exactly as previously described [24]. Strains were inoculated from frozen stocks into LB broth and grown rolling overnight at 30°C. Overnight cultures were diluted into fresh LB to an OD_{600} of 0.08 and grown for 6 hours at 30°C rolling. Subcultured cells were then crosslinked with 1% paraformaldehyde for 20 minutes at room temperature with shaking before being quenched with a 1.2 molar excess of Tris for 10 minutes at room temperature shaking. Cells were then washed twice with TBS (25 mM Tris HCl, pH 7.5 and 125 mM NaCl), and cell pellets were stored at -80°C overnight. Pellets were then resuspended to an OD_{600} of 50.0 in lysis buffer (1x FastBreak cell lysis reagent (Promega), 50 µg/mL lysozyme, 1% Triton X-100, 1 mM PMSF, and 1x protease inhibitor cocktail; 100x inhibitor cocktail contained the following: 0.07 mg/mL phosphoramidon (Santa Cruz), 0.006 mg/mL bestatin (MPbiomedicals/Fisher Scientific), 1.67 mg/mL AEBSF (Gold Bio), 0.07 mg/mL pepstatin A (DOT Scientific), 0.07 mg/mL E64 (Gold Bio) suspended in DMSO). Lysis reactions were incubated for 20 mins rocking at room temperature and were then sonicated with a Fisherbrand Model 705 Sonic Dismembrator 6 times for 10 seconds at 1% amplitude, resting on ice for at least 30 seconds between each sonication (yielding sheared DNA fragments of ~200-300 bp). Sonicated lysates were then centrifuged and diluted 1:5 in IP buffer (50 mM HEPES NaOH pH 7.5, 150 mM NaCl, 1 mM EDTA, and 1% Triton X-100). A sample of diluted lysate was collected to permit quantification of input DNA (see below). 1 mL of diluted lysate was then incubated with end-over-end mixing at room temperature with Pierce anti-DYKDDDDK magnetic agarose equilibrated in IP buffer. Supernatant was then removed using a magnetic separation rack. The magnetic agarose was then washed twice with IP Buffer for 1 minute, once with Wash Buffer 1 (50 mM HEPES NaOH pH 7.5, 1 mM EDTA, 1% Triton X-100, 500 mM NaCl, and 0.1% SDS) for 5 minutes, once with Wash Buffer 2 (10 mM Tris HCl pH 8.0, 250 mM LiCl, 1 mM EDTA, 0.5% NP- 40, and 1% Triton X-100) for 5 minutes, and once with Buffer TE (10 mM tris pH 8.0 and 1 mM EDTA) for 1 minute. To elute protein and DNA off the agarose, it was incubated in SDS elution buffer (50 mM Tris HCl pH 7.5, 10 mM EDTA, and 1% SDS) for 30 minutes at 65°C. The supernatant was then separated from beads using a magnetic separation rack, moved to a new tube, and subjected to digestion with 20 µg Proteinase K in SDS Elution Buffer for 2 hours at 42°C. Crosslinks were then reversed by incubating samples for 6 hours at 65°C. Samples were collected following this incubation for quantification of output DNA. DNA within the samples (input and output) was then purified. Input DNA was diluted 1:100 in buffer EB. Quantitative PCR using iTaq Universal SYBR Green Supermix (Bio-Rad) was then used to measure the abundance of the *chb* promoter in the output (following immunoprecipitation) relative to the input (prior to immunoprecipitation). A standard curve generated from genomic DNA diluted in buffer EB permitted quantification of *chb* abundance. Furthermore, *chb* promoter levels were normalized to levels of a gene that is *not* bound by ChiS, *rpoB*, generating a fold enrichment of the *chb* promoter for each sample.

Western blotting

Strains were inoculated from frozen stocks into LB broth and grown rolling overnight at 30°C. Overnight cultures were washed and resuspended to an OD_{600} of 100.0 in IO and then mixed 1:1 with 2x SDS PAGE sample buffer (200 mM Tris pH 6.8, 25% glycerol, 1.8% SDS, 0.02% Bromophenol Blue, 5% β-mercaptoethanol). Samples were boiled for 10 minutes. For visualizing ChiS-FLAG, 4 uL of sample were separated on a 7.5% SDS PAGE gel. For visualizing RpoA as a loading control, 2 uL of sample were separated on a 15% SDS PAGE gel. Following separation, proteins were electrophoretically transferred to a PVDF membrane. Membranes were then blocked for at least 1 hour in 5% milk and then incubated overnight rocking with either rabbit polyclonal α-FLAG (1:1000, Sigma) or mouse monoclonal α-RpoA (1:1000, Biolegend). Membranes were then washed and incubated for at least 2 hours with either α-rabbit or α-mouse horseradish peroxidase-conjugated secondary antibodies (1:10,000). Blots were then washed and probed with Pierce™ ECL Western Blotting Substrate. Blots were imaged with a ProteinSimple FluorChem R system.

Glucose and Tryptone Growth Curves

Strains were inoculated from frozen stocks into LB broth and grown rolling overnight at 30°C. Overnight cultures were then washed and resuspended in 1X M9 minimal salts + 2 mM $MgSO_4$ + 0.1 mM $CaCl_2$. Cells were inoculated at a starting OD_{600} of 0.001 in 200 µL M9 growth reactions (1X M9 minimal salts + 2 mM $MgSO_4$ + 0.1 mM $CaCl_2$ + 5 µM $FeSO_4$) supplemented with 0.1% glucose or tryptone. The OD_{600} was kinetically monitored every 40 mins in a BioTek H1M plate reader shaking at 30°C.

Statistical comparisons

All statistical comparisons were made by one-way ANOVA with Tukey's multiple comparison test. For ratiometric data (*i.e.*, chitin-induced P_{chb} induction assays, growth assays, transformation frequency assays,

ChIP assays, and colocalization assays) statistical comparisons were performed on log-transformed data. For summary statistics and a complete list of all statistical comparisons, see **S1 dataset**.

ACKNOWLEDGEMENTS
This work was supported by grant R35GM128674 from the National Institutes of Health (to ABD). We would like to thank Dan Kearns, Jake McKinlay, Julia van Kessel, Clay Fuqua, Jen Greenwich, and Courtney Ellison for helpful discussions. We would also like to thank Julia van Kessel for *V. campbellii* DS40M4 and Clay Fuqua for reagents.

AUTHOR CONTRIBUTIONS
V. Green and A. Dalia conceptualized the experiments. Investigation was carried out by V. Green, C. Klancher, and S. Yamamoto. V. Green and A. Dalia wrote the paper and incorporated feedback from all authors.

REFERENCES

1. Silva AJ, Benitez JA. Vibrio cholerae Biofilms and Cholera Pathogenesis. PLoS Negl Trop Dis. 2016;10(2):e0004330. Epub 2016/02/06. doi: 10.1371/journal.pntd.0004330. PubMed PMID: 26845681; PubMed Central PMCID: PMCPMC4741415.
2. Faruque SM, Albert MJ, Mekalanos JJ. Epidemiology, genetics, and ecology of toxigenic Vibrio cholerae. Microbiol Mol Biol Rev. 1998;62(4):1301-14. Epub 1998/12/05. PubMed PMID: 9841673; PubMed Central PMCID: PMCPMC98947.
3. Meibom KL, Li XB, Nielsen AT, Wu CY, Roseman S, Schoolnik GK. The Vibrio cholerae chitin utilization program. Proc Natl Acad Sci U S A. 2004;101(8):2524-9. Epub 2004/02/26. doi: 10.1073/pnas.0308707101. PubMed PMID: 14983042; PubMed Central PMCID: PMCPMC356983.
4. Watnick PI, Kolter R. Steps in the development of a Vibrio cholerae El Tor biofilm. Mol Microbiol. 1999;34(3):586-95. Epub 1999/11/17. doi: 10.1046/j.1365-2958.1999.01624.x. PubMed PMID: 10564499; PubMed Central PMCID: PMCPMC2860543.
5. Meibom KL, Blokesch M, Dolganov NA, Wu CY, Schoolnik GK. Chitin induces natural competence in Vibrio cholerae. Science. 2005;310(5755):1824-7. Epub 2005/12/17. doi: 10.1126/science.1120096. PubMed PMID: 16357262.
6. Sun Y, Bernardy EE, Hammer BK, Miyashiro T. Competence and natural transformation in vibrios. Mol Microbiol. 2013;89(4):583-95. Epub 2013/06/28. doi: 10.1111/mmi.12307. PubMed PMID: 23803158; PubMed Central PMCID: PMCPMC3820095.
7. Blokesch M. Natural competence for transformation. Curr Biol. 2016;26(21):R1126-R30. Epub 2016/11/09. doi: 10.1016/j.cub.2016.08.058. PubMed PMID: 27825443.
8. Li X, Roseman S. The chitinolytic cascade in Vibrios is regulated by chitin oligosaccharides and a two-component chitin catabolic sensor/kinase. Proc Natl Acad Sci U S A. 2004;101(2):627-31. Epub 2003/12/31. doi: 10.1073/pnas.0307645100. PubMed PMID: 14699052; PubMed Central PMCID: PMCPMC327198.
9. Drescher K, Nadell CD, Stone HA, Wingreen NS, Bassler BL. Solutions to the public goods dilemma in bacterial biofilms. Curr Biol. 2014;24(1):50-5. Epub 2013/12/18. doi: 10.1016/j.cub.2013.10.030. PubMed PMID: 24332540; PubMed Central PMCID: PMCPMC3935403.
10. Wolfe AJ. Glycolysis for Microbiome Generation. Microbiol Spectr. 2015;3(3). Epub 2015/07/18. doi: 10.1128/microbiolspec.MBP-0014-2014. PubMed PMID: 26185089; PubMed Central PMCID: PMCPMC4507297.
11. Gorke B, Stulke J. Carbon catabolite repression in bacteria: many ways to make the most out of nutrients. Nat Rev Microbiol. 2008;6(8):613-24. Epub 2008/07/17. doi: 10.1038/nrmicro1932. PubMed PMID: 18628769.
12. Deutscher J, Francke C, Postma PW. How phosphotransferase system-related protein phosphorylation regulates carbohydrate metabolism in bacteria. Microbiol Mol Biol Rev. 2006;70(4):939-1031. Epub 2006/12/13. doi: 10.1128/MMBR.00024-06. PubMed PMID: 17158705; PubMed Central PMCID: PMCPMC1698508.
13. Kundig W, Ghosh S, Roseman S. Phosphate Bound to Histidine in a Protein as an Intermediate in a Novel Phospho-Transferase System. Proc Natl Acad Sci U S A. 1964;52:1067-74. Epub 1964/10/01. doi: 10.1073/pnas.52.4.1067. PubMed PMID: 14224387; PubMed Central PMCID: PMCPMC300396.
14. Hogema BM, Arents JC, Bader R, Eijkemans K, Yoshida H, Takahashi H, et al. Inducer exclusion in Escherichia coli by non-PTS substrates: the role of the PEP to pyruvate ratio in determining the

phosphorylation state of enzyme IIAGlc. Mol Microbiol. 1998;30(3):487-98. Epub 1998/11/21. doi: 10.1046/j.1365-2958.1998.01053.x. PubMed PMID: 9822815.
15. Houot L, Chang S, Absalon C, Watnick PI. Vibrio cholerae phosphoenolpyruvate phosphotransferase system control of carbohydrate transport, biofilm formation, and colonization of the germfree mouse intestine. Infect Immun. 2010;78(4):1482-94. Epub 2010/02/04. doi: 10.1128/IAI.01356-09. PubMed PMID: 20123708; PubMed Central PMCID: PMCPMC2849402.
16. Leng Y, Vakulskas CA, Zere TR, Pickering BS, Watnick PI, Babitzke P, et al. Regulation of CsrB/C sRNA decay by EIIA(Glc) of the phosphoenolpyruvate: carbohydrate phosphotransferase system. Mol Microbiol. 2016;99(4):627-39. Epub 2015/10/29. doi: 10.1111/mmi.13259. PubMed PMID: 26507976; PubMed Central PMCID: PMCPMC4888959.
17. Maze A, Glatter T, Bumann D. The central metabolism regulator EIIAGlc switches Salmonella from growth arrest to acute virulence through activation of virulence factor secretion. Cell Rep. 2014;7(5):1426-33. Epub 2014/05/20. doi: 10.1016/j.celrep.2014.04.022. PubMed PMID: 24835993.
18. Park S, Park YH, Lee CR, Kim YR, Seok YJ. Glucose induces delocalization of a flagellar biosynthesis protein from the flagellated pole. Mol Microbiol. 2016;101(5):795-808. Epub 2016/05/25. doi: 10.1111/mmi.13424. PubMed PMID: 27218601.
19. Pickering BS, Smith DR, Watnick PI. Glucose-specific enzyme IIA has unique binding partners in the vibrio cholerae biofilm. mBio. 2012;3(6):e00228-12. Epub 2012/11/08. doi: 10.1128/mBio.00228-12. PubMed PMID: 23131828; PubMed Central PMCID: PMCPMC3509428.
20. Yamamoto S, Mitobe J, Ishikawa T, Wai SN, Ohnishi M, Watanabe H, et al. Regulation of natural competence by the orphan two-component system sensor kinase ChiS involves a non-canonical transmembrane regulator in Vibrio cholerae. Mol Microbiol. 2014;91(2):326-47. Epub 2013/11/19. doi: 10.1111/mmi.12462. PubMed PMID: 24236404.
21. Dalia AB, Lazinski DW, Camilli A. Identification of a membrane-bound transcriptional regulator that links chitin and natural competence in Vibrio cholerae. mBio. 2014;5(1):e01028-13. Epub 2014/01/30. doi: 10.1128/mBio.01028-13. PubMed PMID: 24473132; PubMed Central PMCID: PMCPMC3903286.
22. Blokesch M. Chitin colonization, chitin degradation and chitin-induced natural competence of Vibrio cholerae are subject to catabolite repression. Environ Microbiol. 2012;14(8):1898-912. Epub 2012/01/10. doi: 10.1111/j.1462-2920.2011.02689.x. PubMed PMID: 22222000.
23. Yamamoto S, Ohnishi M. Glucose-Specific Enzyme IIA of the Phosphoenolpyruvate:Carbohydrate Phosphotransferase System Modulates Chitin Signaling Pathways in Vibrio cholerae. J Bacteriol. 2017;199(18). Epub 2017/05/04. doi: 10.1128/JB.00127-17. PubMed PMID: 28461445; PubMed Central PMCID: PMCPMC5573088.
24. Klancher CA, Yamamoto S, Dalia TN, Dalia AB. ChiS is a noncanonical DNA-binding hybrid sensor kinase that directly regulates the chitin utilization program in Vibrio cholerae. Proc Natl Acad Sci U S A. 2020;117(33):20180-9. Epub 2020/07/29. doi: 10.1073/pnas.2001768117. PubMed PMID: 32719134; PubMed Central PMCID: PMCPMC7443906.
25. Klancher CA, Hayes CA, Dalia AB. The nucleoid occlusion protein SlmA is a direct transcriptional activator of chitobiose utilization in Vibrio cholerae. PLoS Genet. 2017;13(7):e1006877. Epub 2017/07/07. doi: 10.1371/journal.pgen.1006877. PubMed PMID: 28683122; PubMed Central PMCID: PMCPMC5519180.
26. Presper KA, Wong CY, Liu L, Meadow ND, Roseman S. Site-directed mutagenesis of the phosphocarrier protein. IIIGlc, a major signal-transducing protein in Escherichia coli. Proc Natl Acad Sci U S A. 1989;86(11):4052-5. Epub 1989/06/01. doi: 10.1073/pnas.86.11.4052. PubMed PMID: 2657735; PubMed Central PMCID: PMCPMC287386.
27. Feucht BU, Saier MH, Jr. Fine control of adenylate cyclase by the phosphoenolpyruvate:sugar phosphotransferase systems in Escherichia coli and Salmonella typhimurium. J Bacteriol. 1980;141(2):603-10. Epub 1980/02/01. doi: 10.1128/JB.141.2.603-610.1980. PubMed PMID: 6245052; PubMed Central PMCID: PMCPMC293665.
28. Bettenbrock K, Sauter T, Jahreis K, Kremling A, Lengeler JW, Gilles ED. Correlation between growth rates, EIIACrr phosphorylation, and intracellular cyclic AMP levels in Escherichia coli K-12. J Bacteriol. 2007;189(19):6891-900. Epub 2007/08/07. doi: 10.1128/JB.00819-07. PubMed PMID: 17675376; PubMed Central PMCID: PMCPMC2045212.
29. Shimada T, Fujita N, Yamamoto K, Ishihama A. Novel roles of cAMP receptor protein (CRP) in regulation of transport and metabolism of carbon sources. PLoS One. 2011;6(6):e20081. Epub 2011/06/16. doi: 10.1371/journal.pone.0020081. PubMed PMID: 21673794; PubMed Central PMCID: PMCPMC3105977.

30. Hurley JH, Faber HR, Worthylake D, Meadow ND, Roseman S, Pettigrew DW, et al. Structure of the regulatory complex of Escherichia coli IIIGlc with glycerol kinase. Science. 1993;259(5095):673-7. Epub 1993/01/29. PubMed PMID: 8430315.
31. Seok YJ, Sun J, Kaback HR, Peterkofsky A. Topology of allosteric regulation of lactose permease. Proc Natl Acad Sci U S A. 1997;94(25):13515-9. Epub 1998/02/12. doi: 10.1073/pnas.94.25.13515. PubMed PMID: 9391057; PubMed Central PMCID: PMCPMC28337.
32. Chen S, Oldham ML, Davidson AL, Chen J. Carbon catabolite repression of the maltose transporter revealed by X-ray crystallography. Nature. 2013;499(7458):364-8. Epub 2013/06/19. doi: 10.1038/nature12232. PubMed PMID: 23770568; PubMed Central PMCID: PMCPMC3875231.
33. Lee KJ, Jeong CS, An YJ, Lee HJ, Park SJ, Seok YJ, et al. FrsA functions as a cofactor-independent decarboxylase to control metabolic flux. Nat Chem Biol. 2011;7(7):434-6. Epub 2011/05/31. doi: 10.1038/nchembio.589. PubMed PMID: 21623357.
34. Hayes CA, Dalia TN, Dalia AB. Systematic genetic dissection of chitin degradation and uptake in Vibrio cholerae. Environ Microbiol. 2017;19(10):4154-63. Epub 2017/07/29. doi: 10.1111/1462-2920.13866. PubMed PMID: 28752963; PubMed Central PMCID: PMCPMC5647239.
35. Klancher CA, Minasov G, Podicheti R, Rusch DB, Dalia TN, Satchell KJF, et al. The ChiS-Family DNA-Binding Domain Contains a Cryptic Helix-Turn-Helix Variant. mBio. 2021;12(2). Epub 2021/03/18. doi: 10.1128/mBio.03287-20. PubMed PMID: 33727356.
36. Peterkofsky A, Svenson I, Amin N. Regulation of Escherichia coli adenylate cyclase activity by the phosphoenolpyruvate:sugar phosphotransferase system. FEMS Microbiol Rev. 1989;5(1-2):103-8. Epub 1989/06/01. doi: 10.1016/0168-6445(89)90013-2. PubMed PMID: 2699242.
37. Kang S, Lee KH. Transition of Dephospho-DctD to the Transcriptionally Active State via Interaction with Dephospho-IIA(Glc). mBio. 2022;13(2):e0383921. Epub 2022/03/22. doi: 10.1128/mbio.03839-21. PubMed PMID: 35311533; PubMed Central PMCID: PMCPMC9040800.
38. Lim HC, Bernhardt TG. A PopZ-linked apical recruitment assay for studying protein-protein interactions in the bacterial cell envelope. Mol Microbiol. 2019;112(6):1757-68. Epub 2019/09/25. doi: 10.1111/mmi.14391. PubMed PMID: 31550057; PubMed Central PMCID: PMCPMC7218919.
39. Laloux G, Jacobs-Wagner C. Spatiotemporal control of PopZ localization through cell cycle-coupled multimerization. J Cell Biol. 2013;201(6):827-41. Epub 2013/06/12. doi: 10.1083/jcb.201303036. PubMed PMID: 23751494; PubMed Central PMCID: PMCPMC3678156.
40. Klancher CA, Newman JD, Ball AS, van Kessel JC, Dalia AB. Species-Specific Quorum Sensing Represses the Chitobiose Utilization Locus in Vibrio cholerae. Appl Environ Microbiol. 2020;86(18). Epub 2020/07/12. doi: 10.1128/AEM.00915-20. PubMed PMID: 32651201; PubMed Central PMCID: PMCPMC7480382.
41. Wu R, Zhao M, Li J, Gao H, Kan B, Liang W. Direct regulation of the natural competence regulator gene tfoX by cyclic AMP (cAMP) and cAMP receptor protein (CRP) in Vibrios. Sci Rep. 2015;5:14921. Epub 2015/10/08. doi: 10.1038/srep14921. PubMed PMID: 26442598; PubMed Central PMCID: PMCPMC4595672.
42. Lo Scrudato M, Blokesch M. The regulatory network of natural competence and transformation of Vibrio cholerae. PLoS Genet. 2012;8(6):e1002778. Epub 2012/06/28. doi: 10.1371/journal.pgen.1002778. PubMed PMID: 22737089; PubMed Central PMCID: PMCPMC3380833.
43. Redfield RJ, Cameron AD, Qian Q, Hinds J, Ali TR, Kroll JS, et al. A novel CRP-dependent regulon controls expression of competence genes in Haemophilus influenzae. J Mol Biol. 2005;347(4):735-47. Epub 2005/03/17. doi: 10.1016/j.jmb.2005.01.012. PubMed PMID: 15769466.
44. Cameron AD, Volar M, Bannister LA, Redfield RJ. RNA secondary structure regulates the translation of sxy and competence development in Haemophilus influenzae. Nucleic Acids Res. 2008;36(1):10-20. Epub 2007/11/06. doi: 10.1093/nar/gkm915. PubMed PMID: 17981840; PubMed Central PMCID: PMCPMC2248739.
45. Weng Y, Bina XR, Bina JE. Complete Genome Sequence of Vibrio cholerae O1 El Tor Strain C6706. Microbiol Resour Announc. 2021;10(3). Epub 2021/01/23. doi: 10.1128/MRA.01301-20. PubMed PMID: 33478998; PubMed Central PMCID: PMCPMC8407767.
46. Allue-Guardia A, Echazarreta M, Koenig SSK, Klose KE, Eppinger M. Closed Genome Sequence of Vibrio cholerae O1 El Tor Inaba Strain A1552. Genome Announc. 2018;6(9). Epub 2018/03/03. doi: 10.1128/genomeA.00098-18. PubMed PMID: 29496831; PubMed Central PMCID: PMCPMC5834340.
47. Seed KD, Bodi KL, Kropinski AM, Ackermann HW, Calderwood SB, Qadri F, et al. Evidence of a dominant lineage of Vibrio cholerae-specific lytic bacteriophages shed by cholera patients over a 10-year

period in Dhaka, Bangladesh. mBio. 2011;2(1):e00334-10. Epub 2011/02/10. doi: 10.1128/mBio.00334-10. PubMed PMID: 21304168; PubMed Central PMCID: PMCPMC3037004.
48. Colston SM, Hervey WJt, Horne WC, Haygood MG, Petersen BD, van Kessel JC, et al. Complete Genome Sequence of Vibrio campbellii DS40M4. Microbiol Resour Announc. 2019;8(4). Epub 2019/02/01. doi: 10.1128/MRA.01187-18. PubMed PMID: 30701232; PubMed Central PMCID: PMCPMC6346181.
49. Simpson CA, Podicheti R, Rusch DB, Dalia AB, van Kessel JC. Diversity in Natural Transformation Frequencies and Regulation across Vibrio Species. mBio. 2019;10(6). Epub 2019/12/19. doi: 10.1128/mBio.02788-19. PubMed PMID: 31848285; PubMed Central PMCID: PMCPMC6918086.
50. Thomas R, Fukamizo T, Suginta W. Bioeconomic production of high-quality chitobiose from chitin food wastes using an in-house chitinase from Vibrio campbellii. Bioresources and Bioprocessing. 2022;9(1):86. doi: 10.1186/s40643-022-00574-8.
51. Macfadyen LP, Dorocicz IR, Reizer J, Saier MH, Jr., Redfield RJ. Regulation of competence development and sugar utilization in Haemophilus influenzae Rd by a phosphoenolpyruvate:fructose phosphotransferase system. Mol Microbiol. 1996;21(5):941-52. Epub 1996/09/01. doi: 10.1046/j.1365-2958.1996.441420.x. PubMed PMID: 8885265.
52. Inaoka T, Ochi K. RelA protein is involved in induction of genetic competence in certain Bacillus subtilis strains by moderating the level of intracellular GTP. J Bacteriol. 2002;184(14):3923-30. Epub 2002/06/26. doi: 10.1128/JB.184.14.3923-3930.2002. PubMed PMID: 12081964; PubMed Central PMCID: PMCPMC135162.
53. Wang G, Louis JM, Sondej M, Seok YJ, Peterkofsky A, Clore GM. Solution structure of the phosphoryl transfer complex between the signal transducing proteins HPr and IIA(glucose) of the Escherichia coli phosphoenolpyruvate:sugar phosphotransferase system. EMBO J. 2000;19(21):5635-49. Epub 2000/11/04. doi: 10.1093/emboj/19.21.5635. PubMed PMID: 11060015; PubMed Central PMCID: PMCPMC305802.
54. Titgemeyer F, Mason RE, Saier MH, Jr. Regulation of the raffinose permease of Escherichia coli by the glucose-specific enzyme IIA of the phosphoenolpyruvate:sugar phosphotransferase system. J Bacteriol. 1994;176(2):543-6. Epub 1994/01/01. doi: 10.1128/jb.176.2.543-546.1994. PubMed PMID: 8288553; PubMed Central PMCID: PMCPMC205084.
55. Sondej M, Sun J, Seok YJ, Kaback HR, Peterkofsky A. Deduction of consensus binding sequences on proteins that bind IIAGlc of the phosphoenolpyruvate:sugar phosphotransferase system by cysteine scanning mutagenesis of Escherichia coli lactose permease. Proc Natl Acad Sci U S A. 1999;96(7):3525-30. Epub 1999/03/31. doi: 10.1073/pnas.96.7.3525. PubMed PMID: 10097069; PubMed Central PMCID: PMCPMC22326.
56. Osumi T, Saier MH, Jr. Regulation of lactose permease activity by the phosphoenolpyruvate:sugar phosphotransferase system: evidence for direct binding of the glucose-specific enzyme III to the lactose permease. Proc Natl Acad Sci U S A. 1982;79(5):1457-61. Epub 1982/03/01. doi: 10.1073/pnas.79.5.1457. PubMed PMID: 7041121; PubMed Central PMCID: PMCPMC345992.
57. Matamouros S, Hager KR, Miller SI. HAMP Domain Rotation and Tilting Movements Associated with Signal Transduction in the PhoQ Sensor Kinase. mBio. 2015;6(3):e00616-15. Epub 2015/05/28. doi: 10.1128/mBio.00616-15. PubMed PMID: 26015499; PubMed Central PMCID: PMCPMC4447245.
58. Hariharan P, Guan L. Insights into the inhibitory mechanisms of the regulatory protein IIA(Glc) on melibiose permease activity. J Biol Chem. 2014;289(47):33012-9. Epub 2014/10/10. doi: 10.1074/jbc.M114.609255. PubMed PMID: 25296751; PubMed Central PMCID: PMCPMC4239646.
59. Galinier A, Deutscher J. Sophisticated Regulation of Transcriptional Factors by the Bacterial Phosphoenolpyruvate: Sugar Phosphotransferase System. J Mol Biol. 2017;429(6):773-89. Epub 2017/02/17. doi: 10.1016/j.jmb.2017.02.006. PubMed PMID: 28202392.
60. Miller VL, DiRita VJ, Mekalanos JJ. Identification of toxS, a regulatory gene whose product enhances toxR-mediated activation of the cholera toxin promoter. J Bacteriol. 1989;171(3):1288-93. Epub 1989/03/01. doi: 10.1128/jb.171.3.1288-1293.1989. PubMed PMID: 2646275; PubMed Central PMCID: PMCPMC209743.
61. Dalia AB, Lazinski DW, Camilli A. Characterization of undermethylated sites in Vibrio cholerae. J Bacteriol. 2013;195(10):2389-99. Epub 2013/03/19. doi: 10.1128/JB.02112-12. PubMed PMID: 23504020; PubMed Central PMCID: PMCPMC3650525.
62. Dalia AB. Natural Cotransformation and Multiplex Genome Editing by Natural Transformation (MuGENT) of Vibrio cholerae. Methods Mol Biol. 2018;1839:53-64. Epub 2018/07/27. doi: 10.1007/978-1-4939-8685-9_6. PubMed PMID: 30047054.
63. Schindelin J, Arganda-Carreras I, Frise E, Kaynig V, Longair M, Pietzsch T, et al. Fiji: an open-source platform for biological-image analysis. Nat Methods. 2012;9(7):676-82. Epub 2012/06/30. doi: 10.1038/nmeth.2019. PubMed PMID: 22743772; PubMed Central PMCID: PMCPMC3855844.

64. Ducret A, Quardokus EM, Brun YV. MicrobeJ, a tool for high throughput bacterial cell detection and quantitative analysis. Nat Microbiol. 2016;1(7):16077. Epub 2016/08/31. doi: 10.1038/nmicrobiol.2016.77. PubMed PMID: 27572972; PubMed Central PMCID: PMCPMC5010025.
65. Bartlett TM, Bratton BP, Duvshani A, Miguel A, Sheng Y, Martin NR, et al. A Periplasmic Polymer Curves Vibrio cholerae and Promotes Pathogenesis. Cell. 2017;168(1-2):172-85 e15. Epub 2017/01/14. doi: 10.1016/j.cell.2016.12.019. PubMed PMID: 28086090; PubMed Central PMCID: PMCPMC5287421.

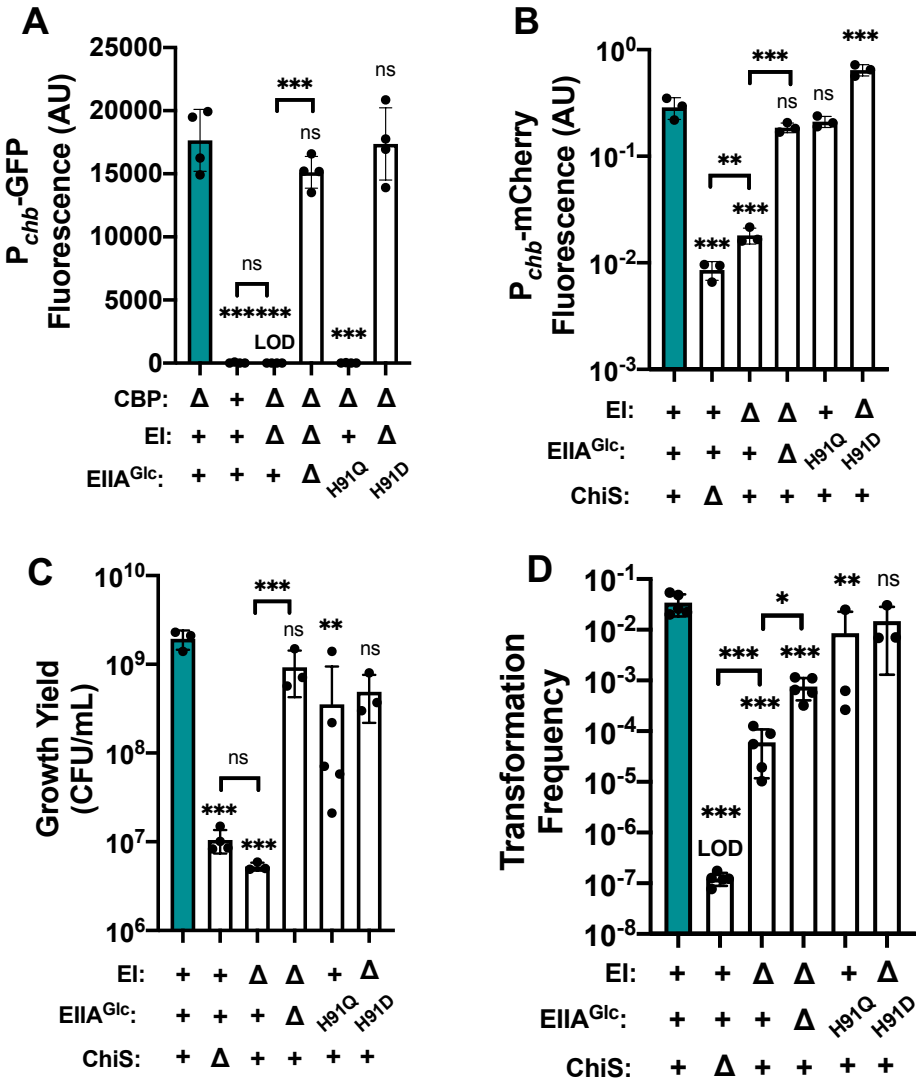

Figure 1. Dephosphorylated EIIA^{Glc} represses ChiS transcriptional activity and downstream behaviors**. (A)** ChiS activation of the *chb* promoter (P_{chb}) was assessed in rich medium (in the absence of chitin) via a P_{chb}-GFP reporter in the indicated strain backgrounds. (**B**) ChiS activation of P_{chb}-mCherry was assessed in the indicated strains after cells were incubated on chitin for 48 hrs. mCherry signal was normalized to a constitutively expressed GFP construct. (**C**) Final growth yield of the indicated strains after a 72 hr incubation in M9 minimal medium containing chitin as the sole carbon source. (**D**) Chitin-induced natural transformation assays of the indicated strains. In all experiments, reactions were supplemented with 5 mM cAMP. Results are from at least three independent biological replicates and shown as the mean ± SD. Statistical comparisons were made by one-way ANOVA with Tukey's multiple comparison test. NS, not significant. *** = $p < 0.001$, ** = $p < 0.01$, * = $p < 0.05$. LOD, limit of detection. Statistical identifiers directly above bars represent comparisons to the parent (teal, first bar).

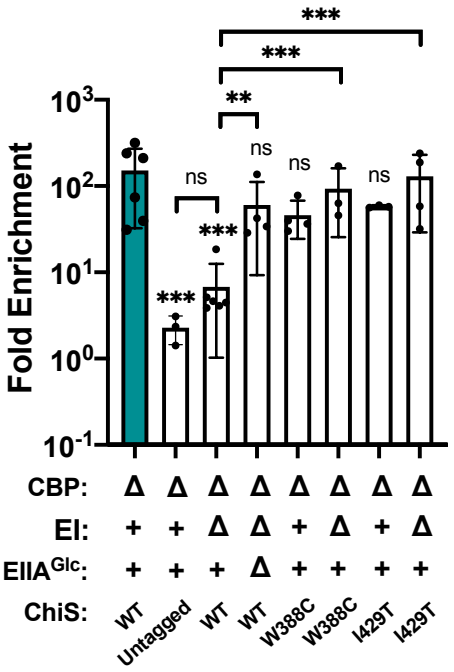

Figure 2. *Dephosphorylated EIIA^{Glc} inhibits the DNA-binding activity of ChiS^{WT} but not ChiS^{W388C} or ChiS^{I429T} in vivo.* ChIP-qPCR assays were performed on the indicated strains to assess ChiS binding to the *chb* promoter (P_{chb}) *in vivo*. Fold enrichment of P_{chb} relative to rpoB is shown. Results are from three independent biological replicates and shown as the mean ± SD. Statistical comparisons were made by one-way ANOVA with Tukey's multiple comparison test. NS, not significant. *** = $p < 0.001$, ** = $p < 0.01$, * = $p < 0.05$. Statistical identifiers directly above bars represent comparisons to the parent (teal, first bar).

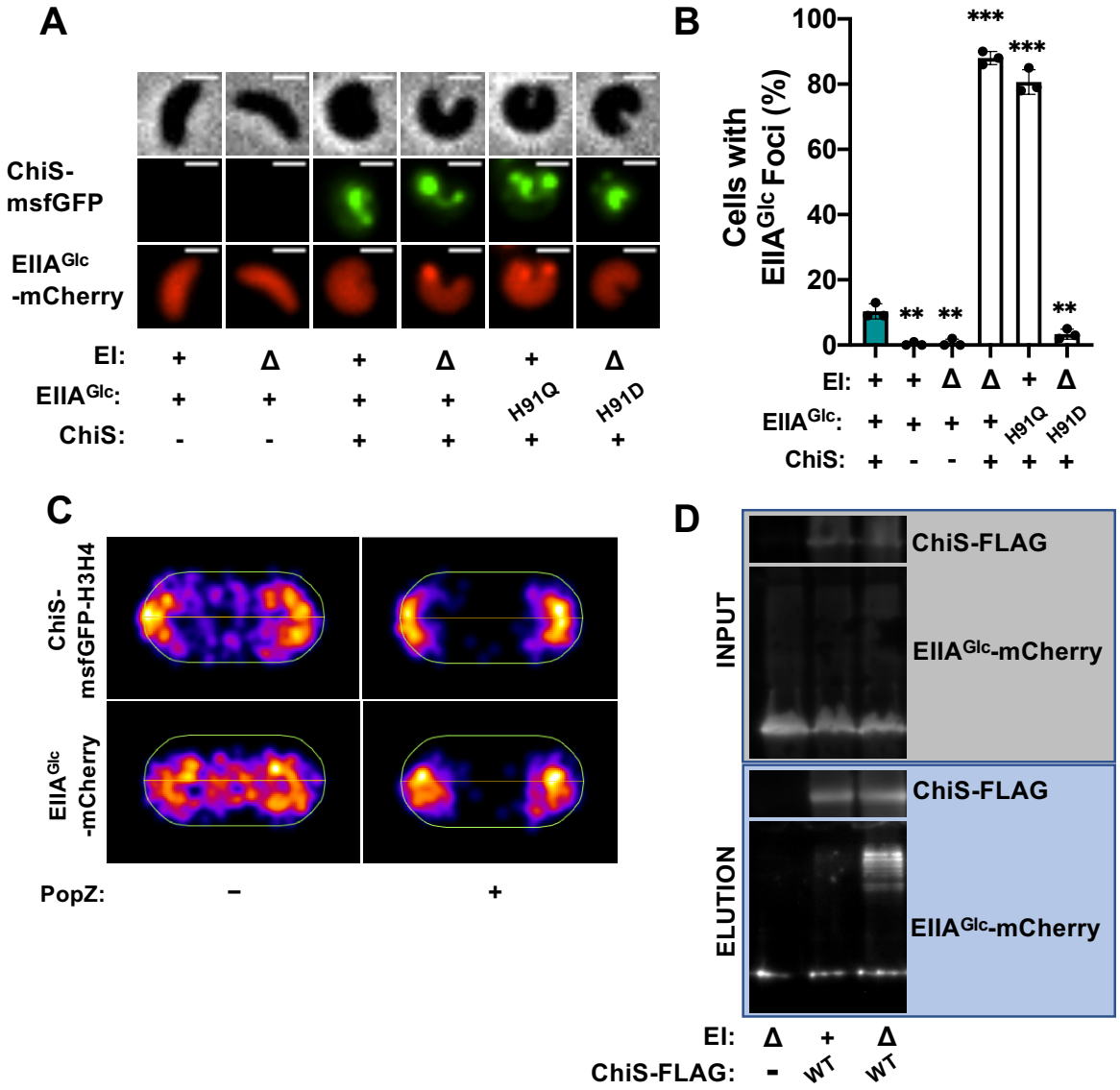

Figure 3. *ChiS interacts with dephosphorylated EIIA^{Glc}.* Colocalization of ChiS and EIIA^{Glc} was assessed in cells either containing or lacking a P$_{tac}$-*chiS-msfGFP* construct and a functional EIIA^{Glc}-*mCherry* fusion at the native locus. For strains containing a P$_{tac}$-*chiS-msfGFP* construct, cultures were supplemented with 20 μM IPTG. (**A**) Representative images of ChiS-msfGFP and EIIA^{Glc}-mCherry localization in the indicated strain backgrounds. Phase (top) is shown to demarcate cell boundaries, GFP fluorescence (middle) shows ChiS-msfGFP localization, and mCherry fluorescence (bottom) shows EIIA^{Glc}-mCherry localization. Scale bar, 1 μm. (**B**) Quantification of the percentage of cells containing EIIA^{Glc} foci in the indicated strains (n = 300 cells analyzed per strain). All EIIA^{Glc} foci observed colocalized with ChiS as shown in **A**. Data are from three independent biological replicates and shown as the mean ± SD. Statistical comparisons were made by one-way ANOVA with Tukey's multiple comparison test. NS, not significant. *** = $p < 0.001$, ** = $p < 0.01$, * = $p < 0.05$. Statistical identifiers directly above bars represent comparisons to the parent (teal, first bar). (**C**) Representative heat maps showing the localization of EIIA^{Glc}-mCherry and ChiS-H3H4-msfGFP foci in ΔEI cells in the presence and absence of PopZ expression. $n \geq 300$ cells analyzed per condition. Data are representative of two independent experiments. (**D**) Representative image of pulldown assays. DSS crosslinked lysates from cells expressing EIIA^{Glc}-mCherry and ChiS-FLAG were immunoprecipitated with anti-FLAG magnetic beads. Bound protein was eluted and protein input (grey box) and elution (blue box) samples were visualized by western blotting. Data are representative of two independent experiments.

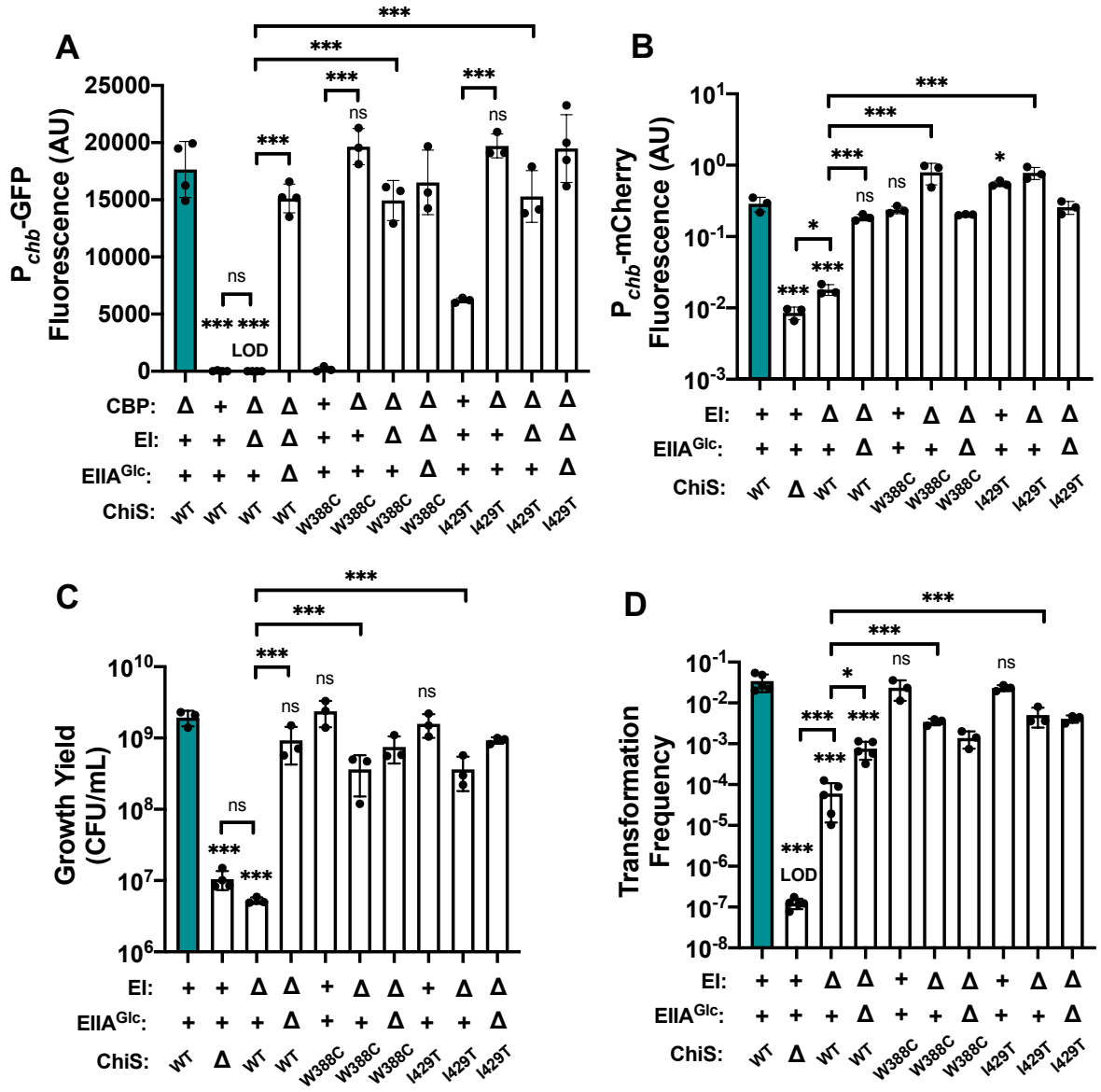

Figure 4. *Dephosphorylated EIIA^{Glc} cannot inhibit the activity of ChiS suppressor alleles*. **(A)** ChiS activation of the *chb* promoter (P_{chb}) was assessed in rich medium (in the absence of chitin) using a P_{chb}-GFP reporter in the indicated strain backgrounds. (**B**) ChiS activation of P_{chb}-mCherry was assessed in the indicated strains after cells were incubated on chitin for 48 hrs. mCherry signal was normalized to a constitutively expressed GFP construct. (**C**) Final growth yield of the indicated strains after a 72 hr incubation in M9 minimal media containing chitin as the sole carbon source. (**D**) Chitin-induced natural transformation assays of the indicated strains. In all experiments, reactions were supplemented with 5 mM cAMP. Results are from at least three independent biological replicates and shown as the mean ± SD. Statistical comparisons were made by one-way ANOVA with Tukey's multiple comparison test. NS, not significant. *** = $p < 0.001$, ** = $p < 0.01$, * = $p < 0.05$. LOD, limit of detection. Statistical identifiers directly above bars represent comparisons to the parent (teal, first bar). The first four bars in each panel are the same data presented in **Fig. 1** and are included here for ease of comparison.

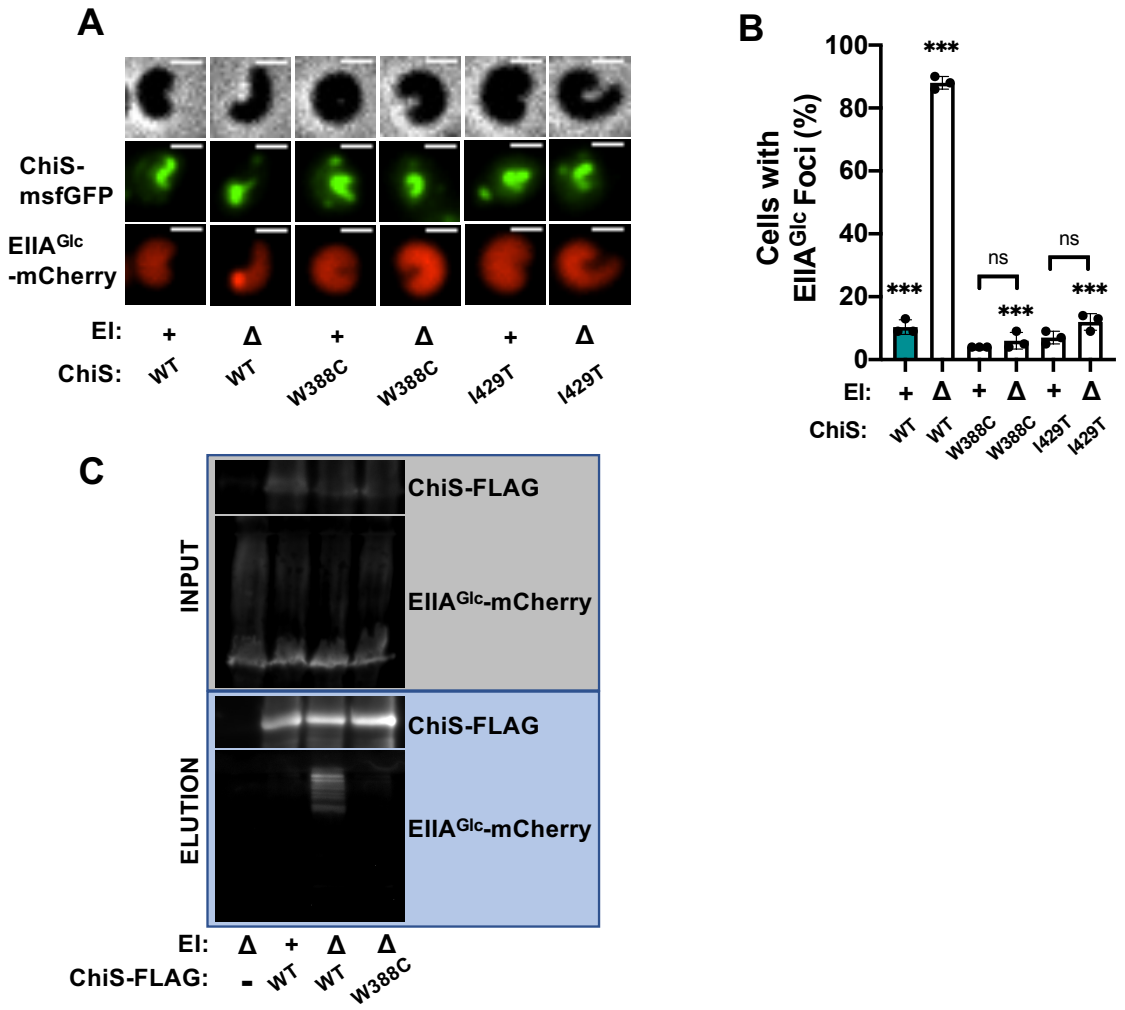

Figure 5. *ChiS suppressor alleles no longer interact with dephosphorylated EIIA^{Glc}.* Colocalization of ChiS and EIIA^{Glc} was assessed in cells containing a P$_{tac}$-*chiS-msfGFP* construct and a functional EIIA^{Glc}-*mCherry* fusion at the native locus. Cultures were supplemented with 20 μM IPTG to induce expression of the indicated ChiS-msfGFP allele. (**A**) Representative images of cells to assess the localization of ChiS-msfGFP and EIIA^{Glc}-mCherry in the indicated strains. Phase (top) is shown to demarcate cell boundaries, GFP fluorescence (middle) shows ChiS-msfGFP localization, and mCherry fluorescence (bottom) shows EIIA^{Glc}-mCherry localization. Scale bar, 1 μm. (**B**) Quantification of the percent of cells containing EIIA^{Glc} foci in the indicated strains (n = 300 cells analyzed per strain). All EIIA^{Glc} foci observed colocalized with ChiS as shown in **A**. Data are from three independent biological replicates and shown as the mean ± SD. Statistical comparisons were made by one-way ANOVA with Tukey's multiple comparison test. NS, not significant. *** = $p < 0.001$, ** = $p < 0.01$, * = $p < 0.05$. Statistical identifiers directly above bars represent comparisons to the parent (teal, first bar). Data for ChiS^{WT} in **B** are the same data shown in **Fig. 2B** and are included here for ease of comparison. (**C**) Representative image of pulldown assays. DSS crosslinked lysates from cells expressing EIIA^{Glc}-mCherry and the indicated allele of ChiS-FLAG were immunoprecipitated with anti-FLAG magnetic beads. Bound protein was eluted and protein input (grey box) and elution (blue box) samples were visualized by western blotting. Data are representative of two independent experiments.

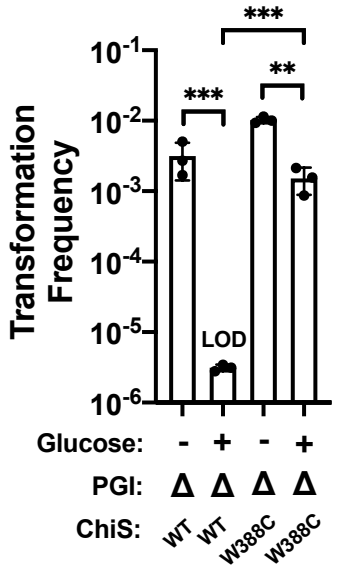

Figure 6. *The ChiS^{W388C} allele confers resistance to glucose-induced CCR of natural transformation***.** Chitin-induced natural transformation assays of the indicated strains. Transformation reactions were supplemented with 0.5% glucose as indicated. All transformation reactions were supplemented with 5 mM cAMP. Results are from at least three independent biological replicates and shown as the mean ± SD. Statistical comparisons were made by one-way ANOVA with Tukey's multiple comparison test. NS, not significant. *** = $p < 0.001$, ** = $p < 0.01$, * = $p < 0.05$. LOD, limit of detection.

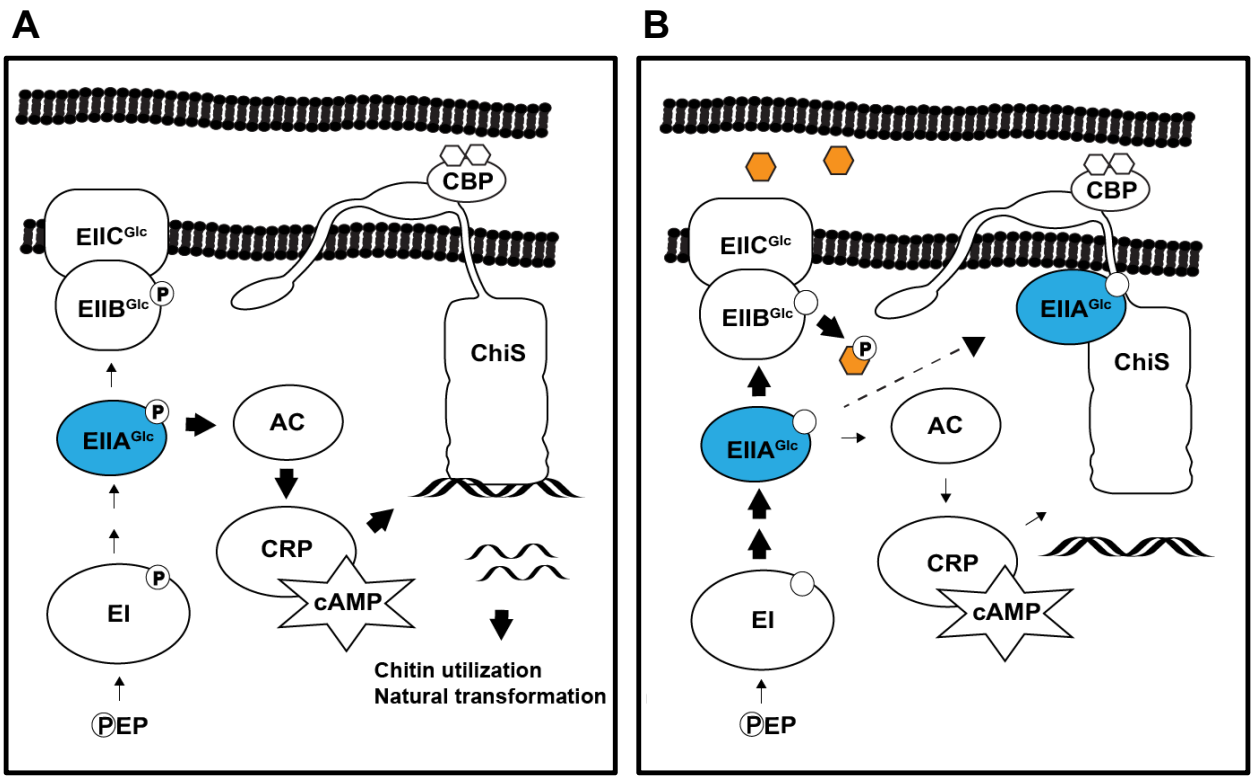

Figure 7. *Model for CCR of the V. cholerae chitin response.* (**A**) In the absence of glucose, phosphate (**P**) accumulates on PTS components due to the absence of a substrate. Thus, EIIA^{Glc} (blue) is phosphorylated and unable to interact with ChiS. When activated by chitin-bound CBP, ChiS binds DNA and promotes the transcription of genes required for natural transformation and chitin utilization. Phospho-EIIA^{Glc} also interacts with adenylate cyclase (AC) to strongly induce its activity, which results in the production of high levels of cAMP. This cAMP complexes with the cAMP receptor protein (CRP) to stimulate both ChiS activity and natural transformation. (**B**) In the presence of glucose (orange hexagon), rapid phosphotransfer through the PTS results in dephosphorylation of EIIA^{Glc}. The absence of phosphorylated EIIA^{Glc} reduces adenylate cyclase activity and resultant CRP-cAMP activity. However, our results demonstrate that CCR due to a reduction in cAMP production cannot account for repression of ChiS activity. Instead, we found that dephospho-EIIA^{Glc} interacts with ChiS to inhibit its DNA-binding activity. Thus, ChiS is unable to activate its target genes, resulting in the loss of chitin utilization and natural transformation.

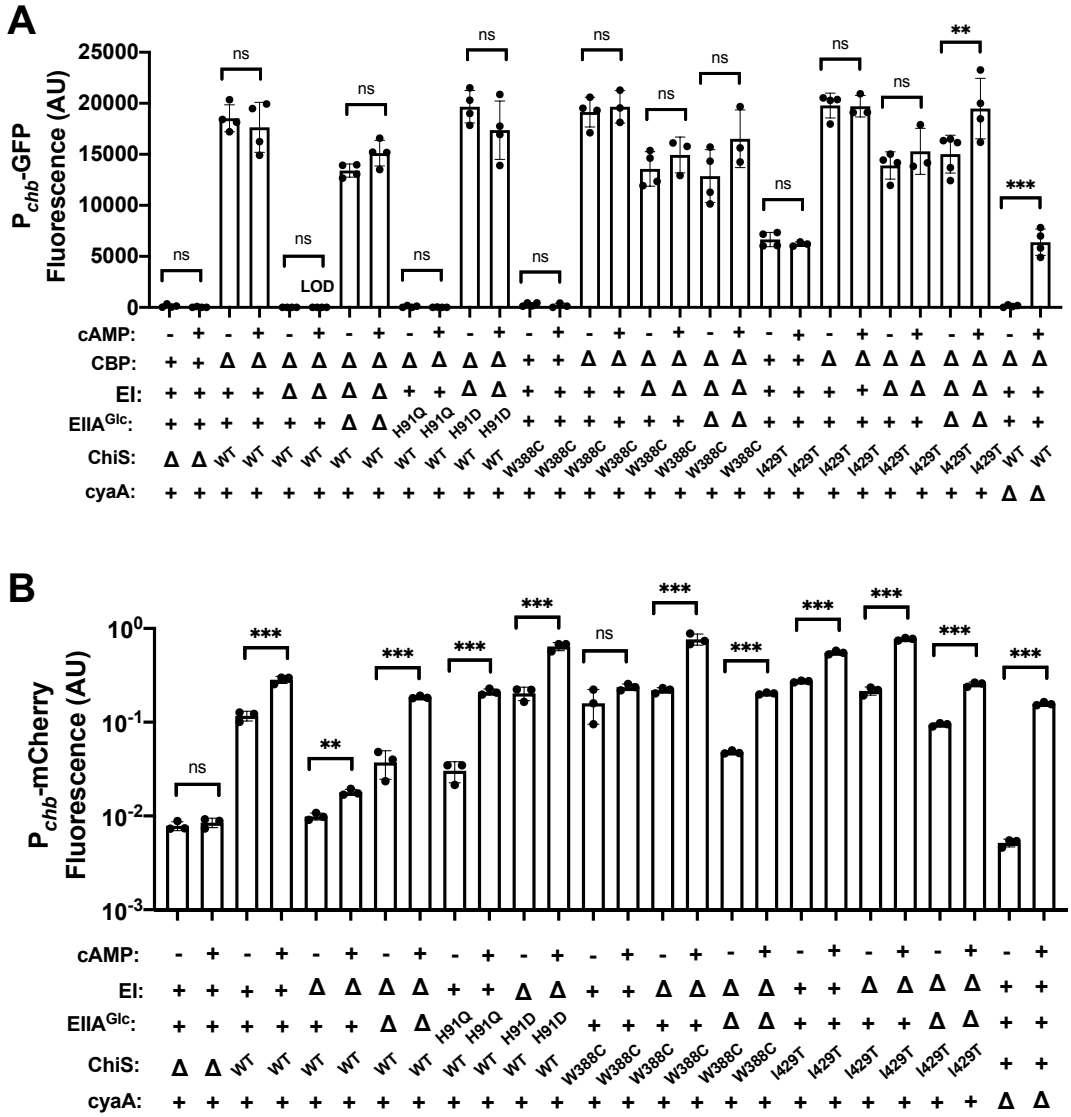

Figure S1. *Dephosphorylated EIIA^{Glc} represses WT but not suppressor ChiS transcriptional activity in the presence or absence of exogenous cAMP*. **(A)** ChiS activation of the *chb* promoter was assessed in rich medium (in the absence of chitin) using a P_{chb}-*GFP* reporter in the indicated strain backgrounds. (**B**) ChiS activation of P_{chb}-*mCherry* was assessed in the indicated strains after cells were incubated on chitin for 48 hrs. mCherry signal was normalized to a constitutively expressed GFP construct. All experiments were performed in the presence or absence of 5 mM exogenous cAMP as indicated. All data for samples where exogenous cAMP was added are identical to that present in **Fig. 1A-B** and are included here for ease of comparison. Results are from at least three independent biological replicates and shown as the mean ± SD. Statistical comparisons were made by one-way ANOVA with Tukey's multiple comparison test. NS, not significant. *** = $p < 0.001$, ** = $p < 0.01$, * = $p < 0.05$.

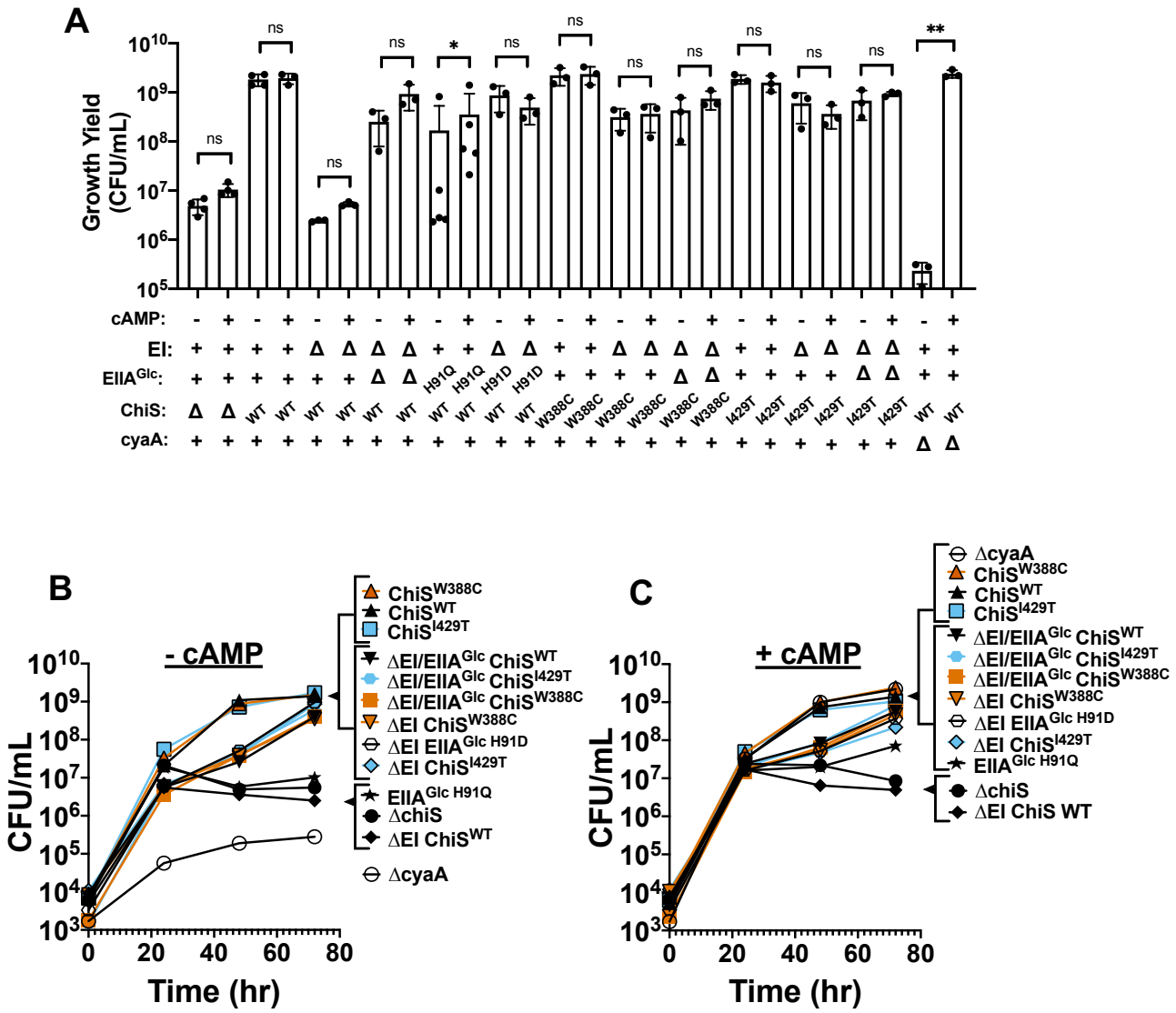

Figure S2. *Dephosphorylated EIIA^{Glc} represses growth on chitin of WT but not suppressor ChiS in the presence or absence of exogenous cAMP*. (**A**) Final growth yield of the indicated strains after a 72 hr incubation in M9 minimal media containing chitin as the sole carbon source. Reactions were supplemented with 5 mM cAMP as indicated. Results are from at least three independent biological replicates and shown as the mean ± SD. Statistical comparisons were made by one-way ANOVA with Tukey's multiple comparison test. NS, not significant. *** = $p < 0.001$, ** = $p < 0.01$, * = $p < 0.05$. Data for reactions supplemented with cAMP are identical to that presented in **Fig. 1C** and are included here for ease of comparison. (**B**-**C**) Representative growth curves of the indicated strains in M9 minimal media containing chitin as the sole carbon source. Reactions either (**B**) lacked exogenous cAMP or (**C**) were supplemented with 5mM cAMP. Strains containing suppressor alleles are colored (orange for W388C, blue for I429T). Data are representative of at least three independent biological replicates.

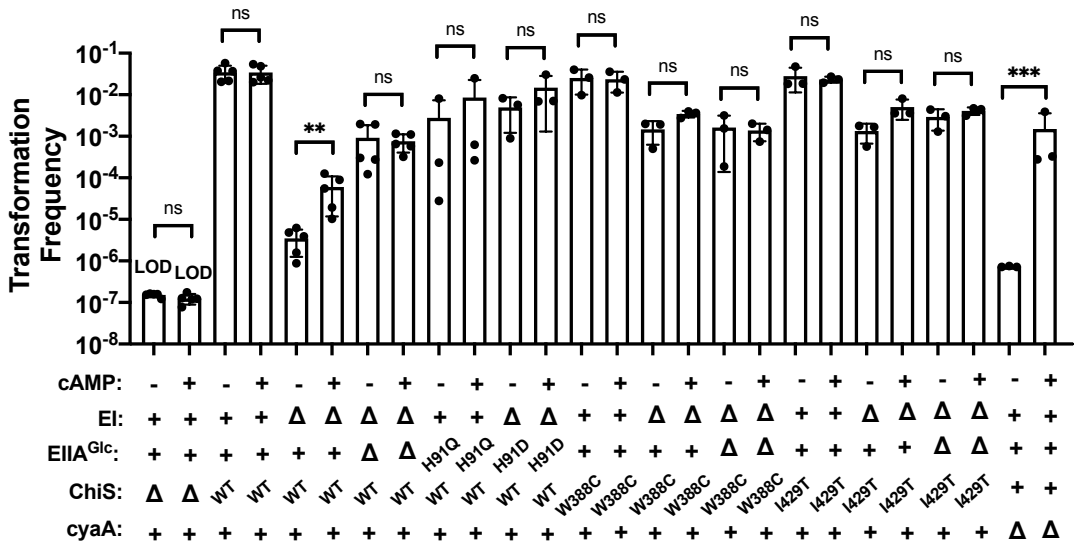

Figure S3. *Dephosphorylated EIIA^{Glc} represses natural transformation of WT but not suppressor ChiS in the presence or absence of exogenous cAMP***.** Chitin-induced natural transformation assays of the indicated strains. Reactions were supplemented with 5 mM exogenous cAMP as indicated. All data for samples where exogenous cAMP was added are identical to that presented in **Fig. 1D** and are included here for ease of comparison. Results are from at least three independent biological replicates and shown as the mean ± SD. Statistical comparisons were made by one-way ANOVA with Tukey's multiple comparison test. NS, not significant. *** = $p < 0.001$, ** = $p < 0.01$, * = $p < 0.05$. LOD, limit of detection.

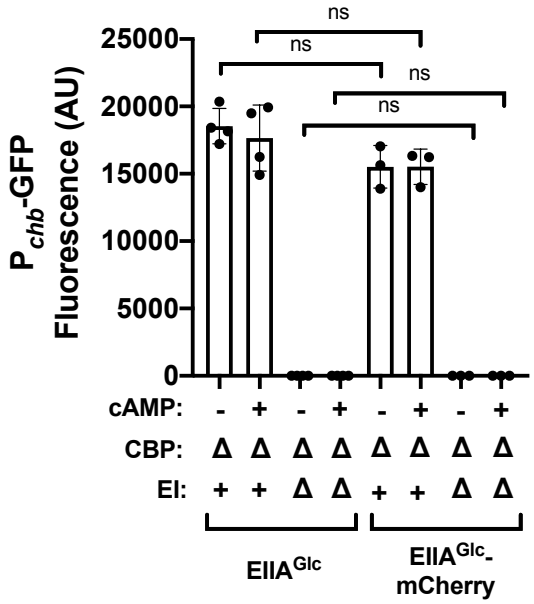

Fig S4. *The $EIIA^{Glc}$-mCherry fusion is fully functional for inhibiting ChiS activity.* ChiS activation of the *chb* promoter was assessed in rich medium (in the absence of chitin) using a P_{chb}-GFP reporter in the indicated strain backgrounds. Results are from three independent biological replicates and shown as the mean ± SD. Statistical comparisons were made by one-way ANOVA with Tukey's multiple comparison test. NS, not significant. *** = $p < 0.001$, ** = $p < 0.01$, * = $p < 0.05$.

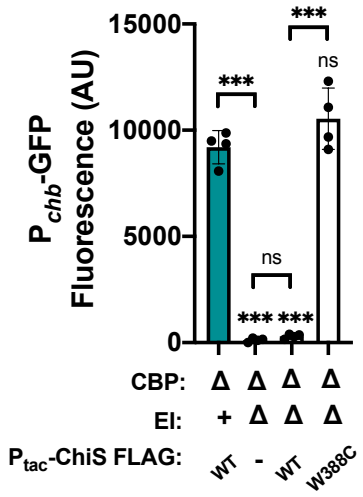

Fig S5. *CCR is maintained in strains overexpressing ChiS.* ChiS activation of the *chb* promoter was assessed in rich medium (in the absence of chitin) using a P_{chb}-GFP reporter in the indicated strain backgrounds. Strains were grown in the present of 1 μM IPTG to induce ChiS-FLAG constructs. Results are from three independent biological replicates and shown as the mean ± SD. Statistical comparisons were made by one-way ANOVA with Tukey's multiple comparison test. Statistical identifiers directly above bars represent comparisons to the parent (teal, first bar). NS, not significant. *** = $p < 0.001$, ** = $p < 0.01$, * = $p < 0.05$.

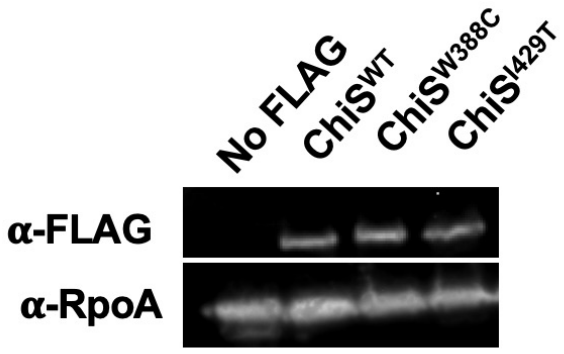

Figure S6. *ChiS suppressor alleles are expressed at WT levels under CCR conditions.* Western blot analysis for ChiS expression. *S*trains contained a ∆EI mutation and the indicated FLAG-tagged ChiS allele. A strain lacking a FLAG-tagged ChiS allele was also included as a negative control (No FLAG). Blots were developed with primary antibodies against FLAG or RpoA as a loading control as indicated. Data are representative of three independent biological replicates.

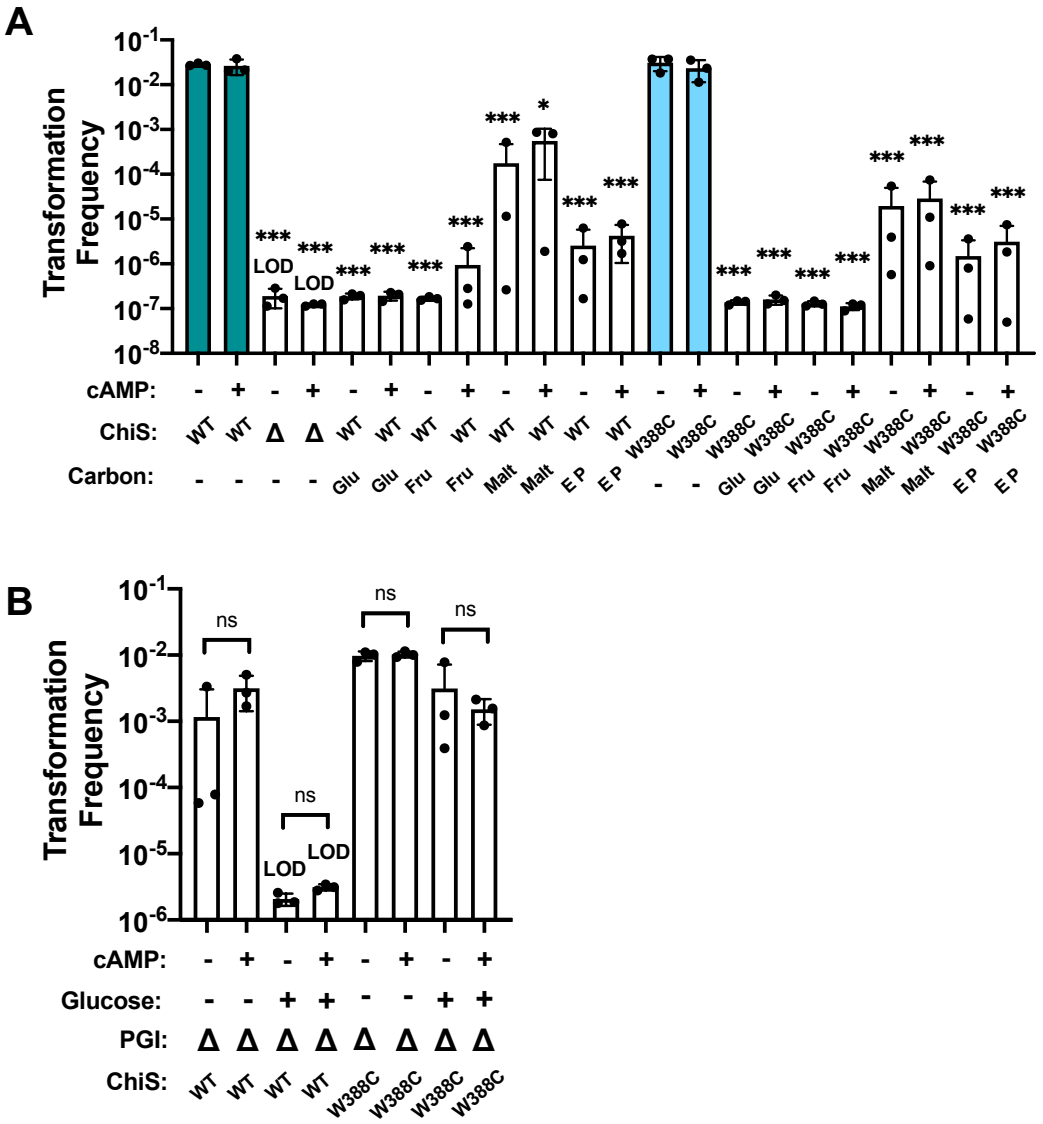

Figure S7. *The ChiS^{W388C} allele confers resistance to glucose-induced CCR of natural transformation in the presence or absence of exogenous cAMP***.** Chitin-induced natural transformation assays of the indicated strains. (**A**) Transformation reactions were supplemented with 0.5% glucose (Glu), fructose (Fru), maltose (Malt), or a mixture of glutamate and proline (E P) as indicated. (**B**) Transformation reactions were supplemented with 0.5% glucose as indicated. Transformation reactions were supplemented with 5 mM cAMP as indicated. Results are from three independent biological replicates and shown as the mean ± SD. Statistical comparisons were made by one-way ANOVA with Tukey's multiple comparison test. NS, not significant. *** = $p < 0.001$, ** = $p < 0.01$, * = $p < 0.05$. LOD, limit of detection. In **A**, statistics directly above data represent comparison to the parent in equivalent cAMP condition (teal, first two bars and blue, fifth and sixth bars). Data for reactions supplemented with exogenous cAMP in **B** are identical to that presented in **Fig. 5** and are included here for ease of comparison.

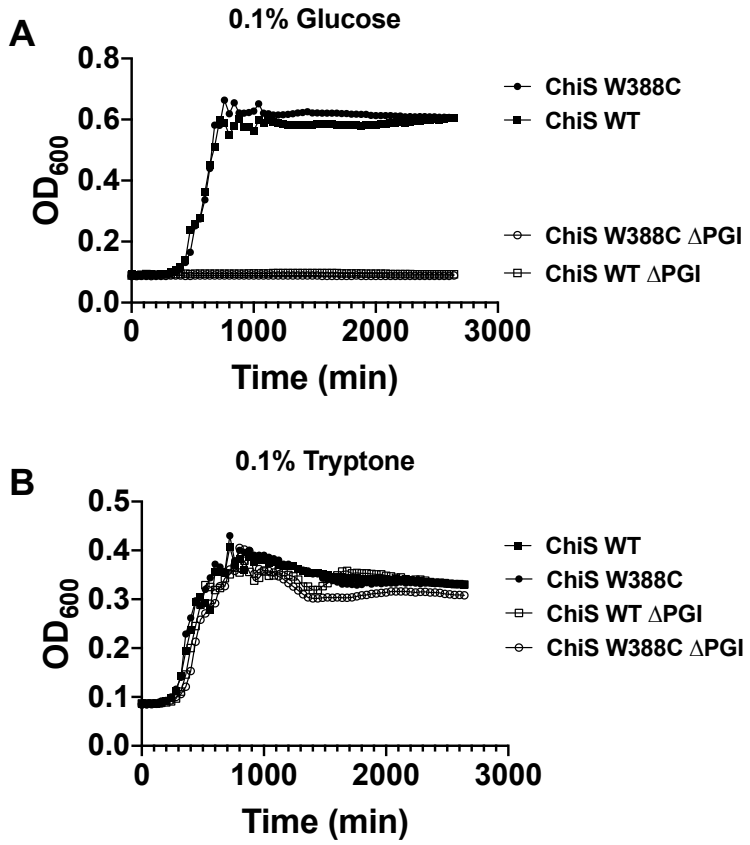

Figure S8. *The ΔPGI mutation prevents growth on glucose but not amino acids.* Representative growth curves of the indicated strains in M9 minimal medium containing 0.1% (**A**) glucose or (**B**) tryptone as the sole carbon source. Data are representative of three independent biological replicates.

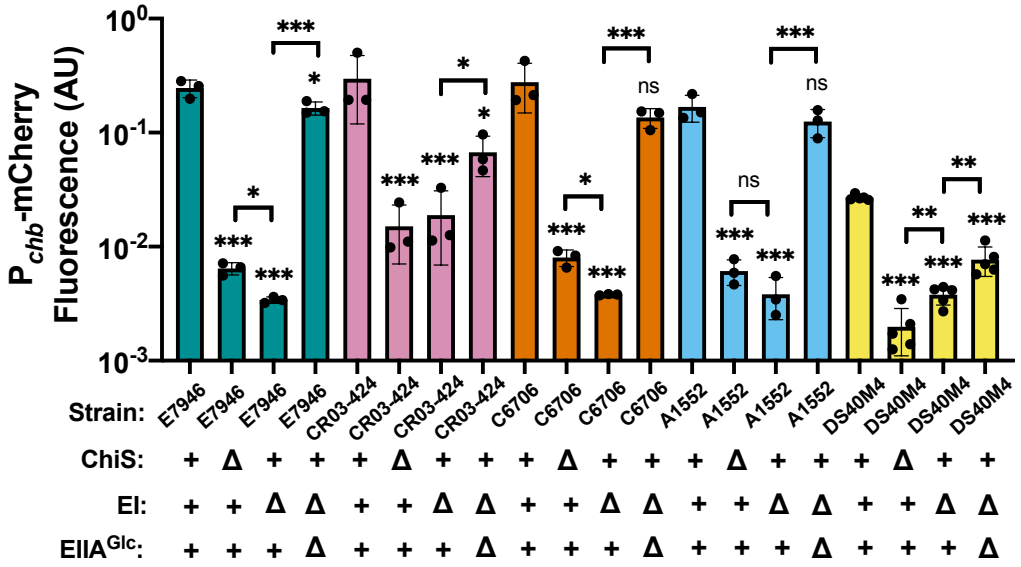

Figure S9. *CCR of ChiS is conserved in diverse* V. cholerae *strains as well as in* Vibrio campbellii**.** ChiS activation of P_{chb}-mCherry was assessed in the indicated strains after cells were incubated on chitin for 48 hrs (*V. cholerae* strains) or 96 hrs (*V. campbellii* DS40M4) in the presence of 5 mM cAMP. mCherry signal was normalized to a constitutively expressed GFP construct. Each strain is shown in a different color, with *V. cholerae* E7946 (the parent for all other strains used in this study) shown in teal, the non-toxigenic environmental *V. cholerae* isolate CR03-424 shown in pink, the toxigenic *V. cholerae* isolate C6706 shown in orange, the toxigenic *V. cholerae* isolate A1552 shown in blue, and the *V. campbellii* DS40M4 strain shown in yellow. Data are from at least three independent biological replicates and are shown as the mean ± SD. Statistical comparisons were made by one-way ANOVA with Tukey's multiple comparison test. NS, not significant. *** = $p < 0.001$, ** = $p < 0.01$, * = $p < 0.05$. Statistical identifiers directly above bars represent comparisons to the parent of the same strain (first column in each color-coded group).

Table S1. Genes referenced in this study

Organism	Gene Name / Product	Gene ID
V. cholerae E7946	*lacZ* / LacZ	VC2338
V. cholerae E7946	*chiS* / ChiS	VC0622
V. cholerae E7946	*cbp* / CBP	VC0620
V. cholerae E7946	*ptsI* / EI	VC0965
V. cholerae E7946	*crr* / $EIIA^{Glc}$	VC0964
V. cholerae E7946	*cyaA* / CyaA	VC0122
V. cholerae E7946	*pgi* / PGI	VC0374
V. cholerae E7946	*crvA* / CrvA	VCA1075
V. campbellii DS40M4	*chiS* / ChiS	DSB67_12445
V. campbellii DS40M4	*ptsI* / EI	DSB67_03835
V. campbellii DS40M4	*crr* / $EIIA^{Glc}$	DSB67_03830

Table S2. Strains used in this study

Strain ID*	Genotype	Reference in Manuscript**
SAD030	*V. cholerae* WT E7946 Sm^R	Parent strain for all *V. cholerae* strains in this study (unless otherwise specified) Fig. 3D, Fig. 5C, Fig. S6 No FLAG
SAD3353 / VEG0562	Δ*lacZ*::Kan^R-P_{chb}-*gfp*; ΔVCA0692::Tm^R-P_{chiS}-*chiS*; Δ*chiS*::$Carb^R$	Fig. 1A, C-D, Fig. 4A, C-D, Fig. S1A, Fig. S2A-C, Fig. S3, Fig. S7A, Fig. S8A-B cbp+ EI+ $EIIA^{Glc}$+ ChiS WT
SAD3354 / VEG0565	Δ*lacZ*::Kan^R-P_{chb}-*gfp*; ΔVCA0692::Tm^R-P_{chiS}-*chiS*; Δ*chiS/cbp*::$Carb^R$	Fig. 1A, Fig. 2, Fig. 3A, Fig. S1A, Fig. S4 Δcbp EI+ $EIIA^{Glc}$+ ChiS WT / Untagged ChiS
SAD3355 / VEG0419	Δ*lacZ*::Kan^R-P_{chb}-*gfp*; ΔVCA0692::Tm^R-P_{chiS}-*chiS*; Δ*chiS/cbp*::$Carb^R$; Δ*ptsI*	Fig. 1A, Fig. 4A, Fig. S1A, Fig. S4 Δcbp ΔEI $EIIA^{Glc}$+ ChiS WT
SAD3356 / VEG0420	Δ*lacZ*::Kan^R-P_{chb}-*gfp*; ΔVCA0692::Tm^R-P_{chiS}-*chiS*; Δ*chiS/cbp*::$Carb^R$; Δ*ptsI/crr*::$Spec^R$	Fig. 1A, Fig. 4A, Fig. S1A Δcbp ΔEI Δ$EIIA^{Glc}$ ChiS WT
SAD3357 / VEG0816	Δ*lacZ*::Kan^R-P_{chb}-*gfp*; ΔVCA0692::Tm^R-P_{chiS}-*chiS*; Δ*chiS/cbp*::$Carb^R$; crr^{H91Q}-$Spec^R$	Fig. 1A, Fig. S1A Δcbp EI+ $EIIA^{Glc}$ H91Q
SAD3358 / VEG1116	Δ*lacZ*::Kan^R-P_{chb}-*gfp*; ΔVCA0692::Tm^R-P_{chiS}-*chiS*; Δ*chiS/cbp*::$Carb^R$; Δ*ptsI*; crr^{H91D}-$Spec^R$	Fig. 1A, Fig. S1A Δcbp ΔEI $EIIA^{Glc}$ H91D
SAD3359 / VEG0757	Δ*lacZ*::Kan^R-P_{chb}-*gfp*; ΔVCA0692::Tm^R-P_{chiS}-$chiS^{W388C}$; Δ*chiS*::$Carb^R$	Fig. 4A, C-D Fig. S1A, Fig. S2A-C, Fig. S3, Fig. S7A, Fig. S8A-B cbp+ EI+ $EIIA^{Glc}$+ ChiS W388C
SAD3360 / VEG0800	Δ*lacZ*::Kan^R-P_{chb}-*gfp*; ΔVCA0692::Tm^R-P_{chiS}-$chiS^{W388C}$; Δ*chiS/cbp*::$Carb^R$	Fig. 4A, Fig. S1A Δcbp EI+ $EIIA^{Glc}$+ ChiS W388C
SAD3361 / VEG0741	Δ*lacZ*::Kan^R-P_{chb}-*gfp*; ΔVCA0692::Tm^R-P_{chiS}-$chiS^{W388C}$; Δ*chiS/cbp*::$Carb^R$; Δ*ptsI*	Fig. 4A, Fig. S1A Δcbp ΔEI $EIIA^{Glc}$+ ChiS W388C

SAD3362 / VEG1121	Δ*lacZ*::Kan^R-P$_{chb}$-*gfp*; ΔVCA0692::Tm^R-P$_{chiS}$-*chiS^{W388C}*; Δ*chiS/cbp*::Carb^R; Δ*ptsI/crr*::Spec^R	Fig. 4A, Fig. S1A Δcbp ΔEI ΔEIIA^{Glc} ChiS W388C
SAD3363 / VEG0765	Δ*lacZ*::Kan^R-P$_{chb}$-*gfp*; ΔVCA0692::Tm^R-P$_{chiS}$-*chiS^{I429T}*; Δ*chiS*::Carb^R	Fig. 4A, C-D, Fig. S1A, Fig. S2A-C, Fig. S3 cbp+ EI+ EIIA^{Glc}+ ChiS I429T
SAD3364 / VEG1052	Δ*lacZ*::Kan^R-P$_{chb}$-*gfp*; ΔVCA0692::Tm^R-P$_{chiS}$-*chiS^{I429T}*; Δ*chiS/cbp*::Carb^R	Fig. 4A, Fig. S1A Δcbp EI+ EIIA^{Glc}+ ChiS I429T
SAD3365 / VEG1004	Δ*lacZ*::Kan^R-P$_{chb}$-*gfp*; ΔVCA0692::Tm^R-P$_{chiS}$-*chiS^{I429T}*; Δ*chiS/cbp*::Carb^R; Δ*ptsI*	Fig. 4A, Fig. S1A Δcbp ΔEI EIIA^{Glc}+ ChiS I429T
SAD3366 / VEG1122	Δ*lacZ*::Kan^R-P$_{chb}$-*gfp*; ΔVCA0692::Tm^R-P$_{chiS}$-*chiS^{I429T}*; Δ*chiS/cbp*::Carb^R; Δ*ptsI/crr*::Spec^R	Fig. 4A, Fig. S1A Δcbp ΔEI ΔEIIA^{Glc} ChiS I429T
SAD3367 / VEG1055	Δ*lacZ*::Kan^R-P$_{chb}$-*gfp*; ΔVCA0692::Tm^R-P$_{chiS}$-*chiS*; Δ*chiS/cbp*::Carb^R; Δ*cyaA*	Fig. S1A Δcbp EI+ EIIA^{Glc}+ ChiS WT ΔcyaA
SAD3368 / VEG0728	Δ*lacZ*::Kan^R-P$_{chb}$-*gfp*; ΔVCA0692::Tm^R-P$_{chiS}$-*chiS^{W388C}*; Δ*chiS*::Carb^R; Δ*ptsI*	Fig. 4C-D, Fig. S2A-C, Fig. S3 ΔEI EIIA^{Glc}+ ChiS W388C
SAD3369 / VEG1125	Δ*lacZ*::Kan^R-P$_{chb}$-*gfp*; ΔVCA0692::Tm^R-P$_{chiS}$-*chiS^{W388C}*; Δ*chiS*::Carb^R; Δ*ptsI/crr*::Spec^R	Fig. 4C-D, Fig. S2A-C, Fig. S3 ΔEI ΔEIIA^{Glc} ChiS W388C
SAD3370 / VEG0736	Δ*lacZ*::Kan^R-P$_{chb}$-*gfp*; ΔVCA0692::Tm^R-P$_{chiS}$-*chiS^{I429T}*; Δ*chiS*::Carb^R; Δ*ptsI*	Fig. 4C-D, Fig. S2A-C, Fig. S3 ΔEI EIIA^{Glc}+ ChiS I429T
SAD3371 / VEG1126	Δ*lacZ*::Kan^R-P$_{chb}$-*gfp*; ΔVCA0692::Tm^R-P$_{chiS}$-*chiS^{I429T}*; Δ*chiS*::Carb^R; Δ*ptsI/crr*::Spec^R	Fig. 4C-D, Fig. S2A-C, Fig. S3 ΔEI ΔEIIA^{Glc} ChiS I429T
SAD3372 / VEG1053	Δ*lacZ*::Kan^R-P$_{chb}$-*gfp*; ΔVCA0692::Tm^R-P$_{chiS}$-*chiS*; Δ*chiS*::Carb^R; Δ*cyaA*	Fig. S2A-C, Fig. S3 EI+ EIIA^{Glc}+ ChiS WT ΔcyaA
SAD3373 / VEG1000	Δ*lacZ*::Kan^R-P$_{chb}$-*mCherry*; igVCA0265-VCA0266::Spec^R-P$_{const2}$-*gfp*; Δ*chiS*::Carb^R	Fig. 1B, Fig. 4B, Fig. S1B, Fig. S9 EI+ EIIA^{Glc}+ ΔchiS E7946
SAD3374 / VEG0997	Δ*lacZ*::Kan^R-P$_{chb}$-*mCherry*; igVCA0265-VCA0266::Spec^R-P$_{const2}$-*gfp*; ΔVCA0692::Tm^R-P$_{chiS}$-*chiS*; Δ*chiS*::Carb^R	Fig. 1B, Fig. 4B, Fig. S1B EI+ EIIA^{Glc}+ ChiS WT
SAD3375 / VEG0974	Δ*lacZ*::Kan^R-P$_{chb}$-*mCherry*; igVCA0265-VCA0266::Spec^R-P$_{const2}$-*gfp*; ΔVCA0692::Tm^R-P$_{chiS}$-*chiS*; Δ*chiS*::Carb^R; Δ*ptsI*	Fig. 1B, Fig. 4B, Fig. S1B ΔEI EIIA^{Glc}+ ChiS WT
SAD3376 / VEG0976	Δ*lacZ*::Kan^R-P$_{chb}$-*mCherry*; igVCA0265-VCA0266::Spec^R-P$_{const2}$-*gfp*; ΔVCA0692::Tm^R-P$_{chiS}$-*chiS*; Δ*chiS*::Carb^R; Δ*ptsI/crr*::Erm^R	Fig. 1B, Fig. 4B, Fig. S1B ΔEI ΔEIIA^{Glc} ChiS WT
SAD3377 / VEG1124	Δ*lacZ*::Kan^R-P$_{chb}$-*mCherry*; igVCA0265-VCA0266::Spec^R-P$_{const2}$-*gfp*; ΔVCA0692::Tm^R-P$_{chiS}$-*chiS*; Δ*chiS*::Carb^R; *crr^{H91Q}*-Erm^R	Fig. 1B, Fig. S1B EI+ EIIA^{Glc} H91Q chiS+
SAD3378 / VEG1118	Δ*lacZ*::Kan^R-P$_{chb}$-*mCherry*; igVCA0265-VCA0266::Spec^R-P$_{const2}$-*gfp*; ΔVCA0692::Tm^R-P$_{chiS}$-*chiS*; Δ*chiS*::Carb^R; Δ*ptsI*; *crr^{H91D}*-Erm^R	Fig. 1B, Fig. S1B ΔEI EIIA^{Glc} H91D chiS+
SAD3379 / VEG1058	Δ*lacZ*::Kan^R-P$_{chb}$-*mCherry*; igVCA0265-VCA0266::Spec^R-P$_{const2}$-*gfp*; ΔVCA0692::Tm^R-P$_{chiS}$-*chiS^{W388C}*; Δ*chiS*::Carb^R	Fig. 4B, Fig. S1B EI+ EIIA^{Glc}+ ChiS W388C

SAD3380 / VEG0975	Δ*lacZ*::Kan^R-P$_{chb}$-*mCherry*; igVCA0265-VCA0266::Spec^R-P$_{const2}$-*gfp*; ΔVCA0692::Tm^R-P$_{chiS}$-*chiS^{W388C}*; Δ*chiS*::Carb^R; Δ*ptsI*	Fig. 4B, Fig. S1B ΔEI EIIA^{Glc}+ ChiS W388C
SAD3381 / VEG0977	Δ*lacZ*::Kan^R-P$_{chb}$-*mCherry*; igVCA0265-VCA0266::Spec^R-P$_{const2}$-*gfp*; ΔVCA0692::Tm^R-P$_{chiS}$-*chiS^{W388C}*; Δ*chiS*::Carb^R; Δ*ptsI/crr*::Erm^R	Fig. 4B, Fig. S1B ΔEI ΔEIIA^{Glc} ChiS W388C
SAD3382 / VEG1091	Δ*lacZ*::Kan^R-P$_{chb}$-*mCherry*; igVCA0265-VCA0266::Spec^R-P$_{const2}$-*gfp*; ΔVCA0692::Tm^R-P$_{chiS}$-*chiS^{I429T}*; Δ*chiS*::Carb^R	Fig. 4B, Fig. S1B EI+ EIIA^{Glc}+ ChiS I429T
SAD3383 / VEG1090	Δ*lacZ*::Kan^R-P$_{chb}$-*mCherry*; igVCA0265-VCA0266::Spec^R-P$_{const2}$-*gfp*; ΔVCA0692::Tm^R-P$_{chiS}$-*chiS^{I429T}*; Δ*chiS*::Carb^R; Δ*ptsI*	Fig. 4B, Fig. S1B ΔEI EIIA^{Glc}+ ChiS I429T
SAD3384 / VEG1146	Δ*lacZ*::Kan^R-P$_{chb}$-*mCherry*; igVCA0265-VCA0266::Spec^R-P$_{const2}$-*gfp*; ΔVCA0692::Tm^R-P$_{chiS}$-*chiS^{I429T}*; Δ*chiS*::Carb^R; Δ*ptsI/crr*::Erm^R	Fig. 4B, Fig. S1B ΔEI ΔEIIA^{Glc} ChiS I429T
SAD3385 / VEG1127	Δ*lacZ*::Kan^R-P$_{chb}$-*mCherry*; igVCA0265-VCA0266::Spec^R-P$_{const2}$-*gfp*; ΔVCA0692::Tm^R-P$_{chiS}$-*chiS*; Δ*chiS*::Carb^R; Δ*cyaA*	Fig. S1B EI+ EIIA^{Glc}+ ChiS WT ΔcyaA
SAD3386 / VEG0755	Δ*lacZ*::Kan^R-P$_{chb}$-*gfp*; Δ*chiS*::Carb^R	Fig. 1C-D, Fig. 4C-D, Fig. S2A-C, Fig. S3, Fig. S7A EI+ EIIA^{Glc}+ ΔchiS
SAD3387 / VEG0753	Δ*lacZ*::Kan^R-P$_{chb}$-*gfp*; ΔVCA0692::Tm^R-P$_{chiS}$-*chiS*; Δ*chiS*::Carb^R; Δ*ptsI*	Fig. 1C-D, Fig. 4C-D, Fig. S2A-C, Fig. S3 ΔEI EIIA^{Glc}+ ChiS WT
SAD3388 / VEG0754	Δ*lacZ*::Kan^R-P$_{chb}$-*gfp*; ΔVCA0692::Tm^R-P$_{chiS}$-*chiS*; Δ*chiS*::Carb^R; Δ*ptsI/crr*::Spec^R	Fig. 1C-D, Fig. 4C-D, Fig. S2A-C, Fig. S3 ΔEI ΔEIIA^{Glc} ChiS WT
SAD3389 / VEG0815	Δ*lacZ*::Kan^R-P$_{chb}$-*gfp*; ΔVCA0692::Tm^R-P$_{chiS}$-*chiS*; Δ*chiS*::Carb^R; *crr^{H91Q}*-Spec^R	Fig. 1C-D, Fig. S2A-C, Fig. S3 EI+ EIIA^{Glc} H91Q chiS+
SAD3390 / VEG1114	Δ*lacZ*::Kan^R-P$_{chb}$-*gfp*; ΔVCA0692::Tm^R-P$_{chiS}$-*chiS*; Δ*chiS*::Carb^R; Δ*ptsI*; *crr^{H91D}*-Spec^R	Fig. 1C-D, Fig. S2A-C, Fig. S3 EI+ EIIA^{Glc} H91D chiS+
SAD3391 / VEG1059	igVCA0265-VCA0266::Carb^R-P$_{BAD}$-*popZ*; Δ*cbp*::Kan^R; *crr-mCherry*-Spec^R	Fig. 3A-B EI+ EIIAGlc+ ChiS-
SAD3392 / VEG1057	igVCA0265-VCA0266::Carb^R-P$_{BAD}$-*popZ*; Δ*cbp*::Kan^R; Δ*ptsI*; *crr-mCherry*-Spec^R	Fig. 3A-B ΔEI EIIAGlc+ ChiS-
SAD3393 / VEG0798	igVCA0265-VCA0266::Carb^R-P$_{BAD}$-*popZ*; ΔVCA0692::Tm^R-P$_{tac}$-*chiS-msfGFP-H3H4*; Δ*cbp*::Kan^R; *crr-mCherry*-Spec^R	Fig. 3A-B, Fig. 5A-B EI+ EIIA^{Glc}+ ChiS WT
SAD3394 / VEG0799	igVCA0265-VCA0266::Carb^R-P$_{BAD}$-*popZ*; ΔVCA0692::Tm^R-P$_{tac}$-*chiS-msfGFP-H3H4*; Δ*cbp*::Kan^R; Δ*ptsI*; *crr-mCherry*-Spec^R	Fig. 3A-B, Fig. 5A-B ΔEI EIIA^{Glc}+ ChiS WT
SAD3395 / VEG1148	igVCA0265-VCA0266::Carb^R-P$_{BAD}$-*popZ*; ΔVCA0692::Tm^R-P$_{tac}$-*chiS^{W388C}-msfGFP-H3H4*; Δ*cbp*::Kan^R; *crr-mCherry*-Spec^R	Fig. 5A-B EI+ ChiS W388C
SAD3396 / VEG1100	igVCA0265-VCA0266::Carb^R-P$_{BAD}$-*popZ*; ΔVCA0692::Tm^R-P$_{tac}$-*chiS^{W388C}-msfGFP-H3H4*; Δ*cbp*::Kan^R; Δ*ptsI*; *crr-mCherry*-Spec^R	Fig. 5A-B ΔEI ChiS W388C
SAD3397 / VEG1150	igVCA0265-VCA0266::Carb^R-P$_{BAD}$-*popZ*; ΔVCA0692::Tm^R-P$_{tac}$-*chiS^{I429T}-msfGFP-H3H4*; Δ*cbp*::Kan^R; *crr-mCherry*-Spec^R	Fig. 5A-B EI+ ChiS I429T

SAD3398 / VEG1136	igVCA0265-VCA0266::Carb^R-P$_{BAD}$-*popZ*; ΔVCA0692::Tm^R-P$_{tac}$-*chiS^{I429T}-msfGFP-H3H4*; Δ*cbp*::Kan^R; Δ*ptsI*; *crr-mCherry*-Spec^R	Fig. 5A-B ΔEI ChiS I429T
SAD3399 / VEG1026	Δ*lacZ*::Kan^R-P$_{chb}$-*gfp*; ΔVCA0692::Tm^R-P$_{chiS}$-*chiS*; Δ*chiS*::Carb^R; Δ*pgi*::Erm^R	Fig. 6, Fig. S7B, Fig. S8A-B ΔPGI ChiS WT
SAD3400 / VEG1031	Δ*lacZ*::Kan^R-P$_{chb}$-*gfp*; ΔVCA0692::Tm^R-P$_{chiS}$-*chiS^{W388C}*; Δ*chiS*::Carb^R; Δ*pgi*::Erm^R	Fig. 5, Fig. S7B, Fig. S8A-B ΔPGI ChiS W388C
SAD3401 / VEG1101	Δ*lacZ*::Kan^R-P$_{chb}$-*gfp*; ΔVCA0692::Tm^R-P$_{chiS}$-*chiS* internal 1X FLAG after E566; Δ*chiS/cbp*::Carb^R	Fig. 2 Δcbp EI+ EIIA^{Glc}+ ChiS WT
SAD3402 / VEG1102	Δ*lacZ*::Kan^R-P$_{chb}$-*gfp*; ΔVCA0692::Tm^R-P$_{chiS}$-*chiS* internal 1X FLAG after E566; Δ*chiS/cbp*::Carb^R; Δ*ptsI*	Fig. 2, Fig. S6 Δcbp ΔEI EIIA^{Glc}+ ChiS WT
SAD3403 / VEG1123	Δ*lacZ*::Kan^R-P$_{chb}$-*gfp*; ΔVCA0692::Tm^R-P$_{chiS}$-*chiS* internal 1X FLAG after E566; Δ*chiS/cbp*::Carb^R; Δ*ptsI/crr*::Spec^R	Fig. 2 Δcbp ΔEI ΔEIIA^{Glc} ChiS WT
SAD3404 / VEG1131	Δ*lacZ*::Kan^R-P$_{chb}$-*gfp*; ΔVCA0692::Tm^R-P$_{chiS}$-*chiS^{W388C}* internal 1X FLAG after E566; Δ*chiS/cbp*::Carb^R	Fig. 2 Δcbp EI+ EIIA^{Glc}+ ChiS W388C
SAD3405 / VEG1132	Δ*lacZ*::Kan^R-P$_{chb}$-*gfp*; ΔVCA0692::Tm^R-P$_{chiS}$-*chiS^{W388C}* internal 1X FLAG after E566; Δ*chiS/cbp*::Carb^R; Δ*ptsI*	Fig. 2, Fig. S6 Δcbp ΔEI EIIA^{Glc}+ ChiS W388C
SAD3406 / VEG1099	Δ*lacZ*::Kan^R-P$_{chb}$-*gfp*; ΔVCA0692::Tm^R-P$_{chiS}$-*chiS^{I429T}* internal 1X FLAG after E566; Δ*chiS/cbp*::Carb^R	Fig. 2 Δcbp EI+ EIIA^{Glc}+ ChiS I429T
SAD3407 / VEG1134	Δ*lacZ*::Kan^R-P$_{chb}$-*gfp*; ΔVCA0692::Tm^R-P$_{chiS}$-*chiS^{I429T}* internal 1X FLAG after E566; Δ*chiS/cbp*::Carb^R; Δ*ptsI*	Fig. 2, Fig. S6 Δcbp ΔEI EIIA^{Glc}+ ChiS I429T
SAD3408 / VEG1133	Δ*lacZ*::Kan^R-P$_{chb}$-*gfp*; ΔΔ*chiS/cbp*::Carb^R; ΔVCA0692::Tm^R-P$_{chiS}$-*chiS*; *crr-mCherry*-Spec^R	Fig. S4 Δcbp EI+ EIIA^{Glc}-mCherry
SAD3409 / VEG0797	Δ*lacZ*::Kan^R-P$_{chb}$-*gfp*; Δ*chiS/cbp*::Carb^R; ΔVCA0692::Tm^R-P$_{chiS}$-*chiS*; Δ*ptsI*; *crr-mCherry*-Spec^R	Fig. S4 Δcbp ΔEI EIIA^{Glc}-mCherry
SAD3428 / VEG1220	igVCA0265-VCA0266::Carb^R-P$_{BAD}$-*popZ*; ΔVCA0692::Tm^R-P$_{tac}$-*chiS-msfGFP-H3H4*; Δ*cbp*::Kan^R; Δ*ptsI*; *crr-mCherry*-Spec^R; Δ*crvA*::Zeo^R	Fig. 3C
SAD3442 / VEG1184	ΔVCA0692::Tm^R-P$_{tac}$-*chiS^{I429T}-msfGFP-H3H4*; Δ*ptsI*; *crr-mCherry*-Spec^R; Δ*cbp*::Kan^R; igVCA0265-VCA0266::Carb^R-P$_{BAD}$-*popZ*	Fig. 5A-B ΔEI ChiS W388C
SAD3443 / VEG0801	Δ*cbp*::Kan^R; *crr^{H91Q}-mCherry*-Spec^R ΔVCA0692::Tm^R-P$_{tac}$-*chiS-msfGFP-H3H4*; igVCA0265-VCA0266::Carb^R-P$_{BAD}$-*popZ*	Fig. 3A-B EI+ EIIA^{Glc} H91Q ChiS+
SAD3444 / VEG0804	Δ*cbp*::Kan^R; Δ*ptsI*; *crr^{H91D}-mCherry*-Spec^R; ΔVCA0692::Tm^R-P$_{tac}$-*chiS-msfGFP-H3H4*; igVCA0265-VCA0266::Carb^R-P$_{BAD}$-*popZ*	Fig. 3A-B ΔEI EIIA^{Glc} H91D ChiS+
SAD3445 / VEG1303	Δ*ptsI*; *crr-mCherry*-Spec^R; Δ*chiS/cbp*::Carb^R; pMMB67EH *tfoX qstR* Cm^R; Δ*lacZ*::Kan^R-P$_{chb}$-*gfp*	Fig. 3D, Fig. 5C, Fig. S5 ΔCBP ΔEI ChiS -
SAD3446 / VEG1301	*crr-mCherry*-Spec^R; Δ*lacZ*::Kan^R-P$_{chb}$-*gfp*; ΔVCA0692::Tm^R-P$_{tac}$-*chiS* internal 1X FLAG after E566; Δ*chiS/cbp*::Carb^R	Fig. 3D, Fig. 5C, Fig. S5 ΔCBP EI+ ChiS WT

SAD3447 / VEG1288	Δ*ptsI*; *crr-mCherry*-Spec^R; Δ*lacZ*::Kan^R-P$_{chb}$-*gfp*; ΔVCA0692::Tm^R-P$_{tac}$-*chiS* internal 1X FLAG after E566; Δ*chiS/cbp*::Carb^R	Fig. 3D, Fig. 5C, Fig. S5 ΔCBP ΔEI ChiS WT
SAD3448 / VEG1321	Δ*ptsI*; *crr-mCherry*-Spec^R; Δ*lacZ*::Kan^R-P$_{chb}$-*gfp*; ΔVCA0692::Tm^R-P$_{tac}$-*chiS^{W388C}* internal 1X FLAG after E566; Δ*chiS/cbp*::Carb^R	Fig. 5C, Fig. S5 ΔCBP ΔEI ChiS W388C
SAD3449 / VEG1289	igVCA0265-VCA0266::Spec^R-P$_{const2}$-*gfp*; Δ*lacZ*::Kan^R-P$_{chb}$-*mCherry*	Fig. S9 E7946 ChiS+ EI+ EIIA^{Glc}+
SAD3450 / VEG1290	Δ*ptsI*::Erm^R; igVCA0265-VCA0266::Spec^R-P$_{const2}$-*gfp*; Δ*lacZ*::Kan^R-P$_{chb}$-*mCherry*	Fig. S9 E7946 ChiS+ ΔEI EIIA^{Glc}+
SAD3451 / VEG1291	Δ*ptsI/crr*::Erm^R; igVCA0265-VCA0266::Spec^R-P$_{const2}$-*gfp*; Δ*lacZ*::Kan^R-P$_{chb}$-*mCherry*	Fig. S9 E7946 ChiS+ ΔEI ΔEIIA^{Glc}
SAD3452 / VEG1322	*V. cholerae* CR03-424 Δ*chiS*::Carb^R; ΔVCA0692::Spec^R-P$_{const2}$-*gfp*; Δ*lacZ*::Kan^R-P$_{chb}$-*mCherry*	Fig. S9 CR03-424 ΔchiS EI+ EIIA^{Glc}+
SAD3453 / VEG1262	*V. cholerae* CR03-424 ΔVCA0692::Spec^R-P$_{const2}$-*gfp*; Δ*lacZ*::Kan^R-P$_{chb}$-*mCherry*	Fig. S9 CR03-424 ChiS+ EI+ EIIA^{Glc}+
SAD3454 / VEG1269	*V. cholerae* CR03-424 Δ*ptsI*::Erm^R; ΔVCA0692::Spec^R-P$_{const2}$-*gfp*; Δ*lacZ*::Kan^R-P$_{chb}$-*mCherry*	Fig. S9 CR03-424 ChiS+ ΔEI EIIA^{Glc}+
SAD3455 / VEG1271	*V. cholerae* CR03-424 Δ*ptsI/crr*::Erm^R; ΔVCA0692::Spec^R-P$_{const2}$-*gfp*; Δ*lacZ*::Kan^R-P$_{chb}$-*mCherry*	Fig. S9 CR03-424 ChiS+ ΔEI ΔEIIA^{Glc}
SAD3456 / VEG1265	*V. cholerae* C6706 Δ*chiS*::Carb^R; igVCA0265-VCA0266::Spec^R-P$_{const2}$-*gfp*; Δ*lacZ*::Kan^R-P$_{chb}$-*mCherry*	Fig. S9 C6706 ΔchiS EI+ EIIA^{Glc}+
SAD3457 / VEG1250	*V. cholerae* C6706 igVCA0265-VCA0266::Spec^R-P$_{const2}$-*gfp*; Δ*lacZ*::Kan^R-P$_{chb}$-*mCherry*	Fig. S9 C6706 ChiS+ EI+ EIIA^{Glc}+
SAD3458 / VEG1255	*V. cholerae* C6706 Δ*ptsI*::Erm^R; igVCA0265-VCA0266::Spec^R-P$_{const2}$-*gfp*; Δ*lacZ*::Kan^R-P$_{chb}$-*mCherry*	Fig. S9 C6706 ChiS+ ΔEI EIIA^{Glc}+
SAD3459 / VEG1259	*V. cholerae* C6706 Δ*ptsI/crr*::Erm^R; igVCA0265-VCA0266::Spec^R-P$_{const2}$-*gfp*; Δ*lacZ*::Kan^R-P$_{chb}$-*mCherry*	Fig. S9 C6706 ChiS+ ΔEI ΔEIIA^{Glc}
SAD3460 / VEG1266	*V. cholerae* A1552 Δ*chiS*::Carb^R; igVCA0265-VCA0266::Spec^R-P$_{const2}$-*gfp*; Δ*lacZ*::Kan^R-P$_{chb}$-*mCherry*	Fig. S9 A1552 ΔchiS EI+ EIIA^{Glc}+
SAD3461 / VEG1251	*V. cholerae* A1552 igVCA0265-VCA0266::Spec^R-P$_{const2}$-*gfp*; Δ*lacZ*::Kan^R-P$_{chb}$-*mCherry*	Fig. S9 A1552 ChiS+ EI+ EIIA^{Glc}+

SAD3462 / VEG1256	*V. cholerae* A1552 Δ*ptsI*::Erm^R; igVCA0265-VCA0266::Spec^R-P$_{const2}$-*gfp*; Δ*lacZ*::Kan^R-P$_{chb}$-*mCherry*	Fig. S9 A1552 ChiS+ ΔEI EIIA^{Glc}+
SAD3463 / VEG1260	*V. cholerae* A1552 Δ*ptsI/crr*::Erm^R; igVCA0265-VCA0266::Spec^R-P$_{const2}$-*gfp*; Δ*lacZ*::Kan^R-P$_{chb}$-*mCherry*	Fig. S9 A1552 ChiS+ ΔEI ΔEIIA^{Glc}
SAD3464 / VEG1300	*V. campbellii* DS40M4 pMMB67EH *tfoX* Gent^R	DS40M4 Parent for all *V. campbellii* strains used in this study
SAD3465 / VEG1315	*V. campbellii* DS40M4 Δ*chiS*::Erm^R; igDSB10880_10885::Spec^R-P$_{const2}$-*gfp*; igDSB08575_08580::Kan^R-P$_{chb}$-*mCherry*; pMMB67EH *tfoX* Gent^R	Fig. S9 DS40M4 ΔchiS EI+ EIIA^{Glc}+
SAD3466 / VEG1320	*V. campbellii* DS40M4 igDSB10880_10885::Spec^R-P$_{const2}$-*gfp*; igDSB08575_08580::Kan^R-P$_{chb}$-*mCherry*; pMMB67EH *tfoX* Gent^R	Fig. S9 DS40M4 ChiS+ EI+ EIIA^{Glc}+
SAD3467 / VEG1316	*V. campbellii* DS40M4 Δ*ptsI*::Erm^R; igDSB10880_10885::Spec^R-P$_{const2}$-*gfp*; igDSB08575_08580::Kan^R-P$_{chb}$-*mCherry*; pMMB67EH *tfoX* Gent^R	Fig. S9 DS40M4 ChiS+ ΔEI EIIA^{Glc}+
SAD3468 / VEG1317	*V. campbellii* DS40M4 Δ*ptsI/crr*::Erm^R; igDSB10880_10885::Spec^R-P$_{const2}$-*gfp*; igDSB08575_08580::Kan^R-P$_{chb}$-*mCherry*; pMMB67EH *tfoX* Gent^R	Fig. S9 DS40M4 ChiS+ ΔEI ΔEIIA^{Glc}

**Double identifiers under 'Strain ID' refer to the same strain that has been stocked in two independent strain collections.*

***'Reference in Manuscript' describes the figures in which this strain is found and the relevant genotype used in those figures to refer to the strain.*

Table S3. Primers used in this study

Primers for SOE deletions		
Primer	**Sequence**	**Description**
ABD123	ATTCCGGGGATCCGTCGAC	Antibiotic resistance cassette F
ABD124	TGTAGGCTGGAGCTGCTTC	Antibiotic resistance cassette R
ABD767	TTAATTTGGATCCCTGCGACACTC	ΔchiS F1 for Up arm
ABD768	gtcgacggatccccggaatCAAAAAACGTGAGGAGA ATGCC	ΔchiS R1 for Up arm
ABD769	gaagcagctccagcctacaTTCTTGAGCATTGCAAAG AAGC	ΔchiS F2 for Down arm
ABD770	CTGGAACGAATGAAGAAGTCCAG	ΔchiS R2 for Down arm
VGP0199	TCAAACAAAGGCTGACTGAATC	ΔchiS detect R
ABD796	TTAGAATCTGCGCCAGAAGCG	Δcbp F1 for Up arm
ABD797	gtcgacggatccccggaatCATAGCTGTTCCTTACTA GTTGC	Δcbp R1 for Up arm
ABD798	gaagcagctccagcctacaGTACTGGATCTGAAACC AGTTAAG	Δcbp F2 for Down arm
ABD799	GTATTGCGGAATGACCAGCATG	Δcbp R2 for Down arm
VGP0200	GAACAGTGACCAACCAAATGC	Δcbp detect R
ABD963	GCTTGGATGCTGGCTATACAG	ΔEI F1 for Up arm
ABD966	gtcgacggatccccggaatCATAGCCTTACCTTAAACTG GTC	ΔEI R1 for Up arm
ABD967	gaagcagctccagcctacaTAATTATCGGTTGATACCA AGGAG	ΔEI F2 for Down arm
ABD968	TTGATTAATGTGCAGACGGAGC	ΔEI R2 for Down arm
VGP0096	GATAGTACCGTTAACAGGAGCTAC	ΔEI detect R
VGP0001	TGATTGATCGTGTTGAGCGTG	ΔEIIAGlc F1 for Up arm
BBC066	gtcgacggatccccggaatCATTGTGTCATGCTCCTAA CG	ΔEIIAGlc R1 for Up arm
BBC067	gaagcagctccagcctacaACCAAGTAATCGCTTGGTT CG	ΔEIIAGlc F2 for Down arm
BBC068	GGTCGCGATACGCAGATTC	ΔEIIAGlc R2 for Down arm
VGP0100	CGTCATGCTCAGCAGTATGTG	ΔEIIAGlc detect R
BBC040	TTGATCGCCGTTTCTAACTTGG	ΔcyaA F1 for Up arm
BBC041	gtcgacggatccccggaatCAAGTTTGCTTCCCTGATAT G	ΔcyaA R1 for Up arm
BBC042	gaagcagctccagcctacaTAACTCGTTGACGTCTCAG G	ΔcyaA F2 for Down arm
BBC043	CTTGCAGCGACGAGCATTTTAG	ΔcyaA R2 for Down arm
BBC044	CTGGCTGGCCTCCAAATCAGG	ΔcyaA detect R
BBC1492	AGTGCTGCCAACATTAATGCC	Δpgi F1 for Up arm
BBC1493	gtcgacggatccccggaatCATGGCATCTATCCCGATG	Δpgi R1 for Up arm
BBC1494	gaagcagctccagcctacaTAATTACGCCGAATAACCA ATTG	Δpgi F2 for Down arm
BBC1495	GTTGTACGCCAGAAAATCGCC	Δpgi R2 for Down arm
BBC1496	TAGCGTTGATCACTTTGCC	Δpgi detect R
BBC1782	CAAGCGATGTACGAACGAAC	ΔcrvA F1 for Up arm
BBC1783	gtcgacggatccccggaatCCACATAAAGTGGGAAAGA CAAAC	ΔcrvA R1 for Up arm
BBC1784	gaagcagctccagcctacaGTCAATGGCAATGACACG G	ΔcrvA F2 for Down arm
BBC1785	GCTTGACGTTGTTGCTTACTGG	ΔcrvA R2 for Down arm

BBC1786	TTTTGTGATGGCTGGATGTCG	ΔcrvA detect R
ABD725	GAAGCAGCTCCAGCCTACA	Detect F for all deletions
VGP0305	ACCAAGAAACCGTAACGTGCTAC	V. campbellii ΔchiS F1 for Up arm
VGP0306	gtcgacggatccccggaatCATTAGCGTGCTTTGCAGTCG	V. campbellii ΔchiS R1 for Up arm
VGP0307	gaagcagctccagcctacaTAACGCAAACCACCAAATATCAG	V. campbellii ΔchiS F2 for Down arm
VGP0308	GATAGTACAACTGCAGTACCTGC	V. campbellii ΔchiS R2 for Down arm
VGP0309	CTAGGTGAAATTTAATCTGCCG	V. campbellii ΔchiS detect R
VGP0295	TTTATCCTCTTGGTCAACGTCC	V. campbellii ΔEI or ΔEI/EIIAGlc F1 for Up arm
VGP0296	gtcgacggatccccggaatCATAGCCTTACCTTAAGTTGGTC	V. campbellii ΔEI or ΔEI/EIIAGlc R1 for Up arm
VGP0297	gaagcagctccagcctacaTAATCAACTAATTCCAATGAGATAGG	V. campbellii ΔEI F2 for Down arm
VGP0298	CTAAACAACGCAAACTCAGCAC	V. campbellii ΔEI R2 for Down arm
VGP0299	GCCTTTCAGTTCAACAGTGTCG	V. campbellii ΔEI detect R
VGP0302	gaagcagctccagcctacaACTCCAGTTCTACGTGTAACTAAG	V. campbellii ΔEI/EIIAGlc F2 for Down arm
VGP0303	ACTATTGCAGTAGTTTACCTAGCC	V. campbellii ΔEI/EIIAGlc R2 for Down arm
VGP0304	TTAGCGGATGAGCTTGACGTTAC	V. campbellii ΔEI/EIIAGlc detect R
Primers for point mutations		
Primer	**Sequence**	**Description**
VGP0105	CTTTTGAAGCTGACATGtGCAGCCGAACGTGTTTC	ChiS W388C F
VGP0106	GAAACACGTTCGGCTGCaCATGTCAGCTTCAAAAG	ChiS W388C R
VGP0144	CATTCGCGAAAAAAccTCGCTGATCAAATCGC	ChiS I429T F
VGP0145	GCGATTTGATCAGCGAggTTTTTTCGCGAATG	ChiS I429T R
VGP0006	CTGTTTGTTCAaTTCGGTATCG	EIIAGlc H91Q F
VGP0012	CGATACCGAAtTGAACAAACAG	EIIAGlc H91Q R
VGP0002	CTGTTTGTTgAtTTCGGTATCGAC	EIIAGlc H91D F
VGP0003	GTCGATACCGAAaTcAACAAACAG	EIIAGlc H91D R
Primers for ChIP-qPCR		
Primer	**Sequence**	**Description**
BBC989	GCATCTAGGTTTTGACGTTTTTAACG	Pchb F
BBC990	AACACTCTCCAAGACCTACCTC	Pchb R
ABD132	CTGTCTCAAGCCGGTTACAA	rpoB F
ABD133	TTTCTACCAGTGCAGAGATGC	rpoB R
Primers for reporter constructs		
Primer	**Sequence**	**Description**
VGP0093	tccaccacttccacctgcCTTGGTCACGCGTAGGATCGG	EIIAGlc-C terminal tag R1
VGP0094	gcaggtggagcaggtggaTAATCGCTTGGTTCGATTTAAAAC	EIIAGlc-C terminal tag F2
BBC3222	GCaGGTGGAAGTGGTGGAgtgagcaagggcgaggaggataacatgg	mCherry (middle arm) F
BBC3223	tccacctgctccacctgccttgtacagctcgtccatgccgccggtggag	mCherry (middle arm) R

BBC3230	GCAGTAAATCCGACTTTGGAG	Insert construct at igVCA0265-VCA0266 F1
CKP802	caccatacccacgccgaaacaaAGCATTCTGTTGTTATGCTG	Insert construct at igVCA0265-VCA0266 R1
CKP803	gaagcagctccagcctacaTCATAATTTAAGGCGTTAGCAG	Insert construct at igVCA0265-VCA0266 F2
BBC3231	TCTCATAAACCTCATGGTAGACG	Insert construct at igVCA0265-VCA0266 R2
BBC252	caatttcacacaggatcccgggaggaggtaacgtaATGCGTAAAGGAGAAGAAC	Amplify GFP for inserting after Pconst2 F
BBC254	tgtaggctggagctgcttcTTAGTTGTATAGTTCATCCATGCC	Amplify GFP for inserting after Pconst2 at igVCA0265-VCA0266 or VCA0602 R
BBC3082	ttatacgagccttatgcatgcccgtaaagttatccagcaaccactcatagacctagggcagcagatagggacgacgtggtgttagctgtgCTCATTAGGCACCCCAGGC	Insert Pconst2 promoter upstream of GFP R1
BBC3083	tggataactttacgggcatgcataaggctcgtataatatattcagggagaccacaacggtttccctctacaaataattttgtttaactttCAATTTCACACAGGATCCCGGG	Insert Pconst2 promoter upstream of GFP F2
VGP0281	GGAATGACTATCTCGTAATGGAGAC	Insert construct at *V. campbellii* igDSB67_10880-10885 F1
VGP0282	caccatacccacgccgaaacaaACTTGTTGTGCATTGGAATAACTTG	Insert construct at *V. campbellii* igDSB67_10880-10885 R1
VGP0283	gaagcagctccagcctacaAGACCCATAGCCCAGCAACAAG	Insert construct at *V. campbellii* igDSB67_10880-10885 F2
VGP0284	GAAGTTATCAGTTAGAGCGATACC	Insert construct at *V. campbellii* igDSB67_10880-10885 R2
VGP0287	AAGAAGGTACATTATGGACGCAG	Detect construct at *V. campbellii* igDSB67_10880-10885 R
VGP0288	CAACCTAGTTCAGAGCAAACTTG	Insert construct at *V. campbellii* igDSB67_08575-08580 F1
VGP0289	caccatacccacgccgaaacaaTGATCATGATGTCTTAGAGCGC	Insert construct at *V. campbellii* igDSB67_08575-08580 R1
VGP0290	gaagcagctccagcctacaGCCTCTTAGTTAATCAGCTGAG	Insert construct at *V. campbellii* igDSB67_08575-08580 F2
VGP0291	TATGGTAAGACGCTTGCTCCAC	Insert construct at *V. campbellii* igDSB67_08575-08580 R2
VGP0292	TAGTTAACCCTGCGTTTGGTTG	Detect construct at *V. campbellii* igDSB67_08575-08580 R